2017

Design and Modeling of a Heat Exchanger for Porous Combustor Powered Steam Generators in Automotive Industry

Apratim Dasgupta
University of Central Florida

DESIGN AND MODELLING OF A HEAT EXCHANGER FOR POROUS COMBUSTOR POWERED STEAM GENERATORS IN AUTOMOTIVE INDUSTRY

by

APRATIM DASGUPTA
B. TECH West Bengal University of Technology, 2010

A thesis submitted in partial fulfillment of the requirements
for the degree of Master of Science in Aerospace Engineering
in the Department of Mechanical and Aerospace Engineering
in the College of Engineering and Computer Science
at the University of Central Florida
Orlando, Florida

Spring Term
2017

Major Professor: Nina Orlovskaya

ABSTRACT

A major challenge faced by automobile manufacturers is to achieve reduction of particulate emission to acceptable standards, as the emission standards become more and more stringent. One of the ecologically friendly options to reduce emissions is to develop external combustion in a steam engine as a replacement of the internal combustion engine. There are multiple factors, other than pollution that need to be considered for developing a substitute for Internal Combustion Engine, like specific power, throttle response, torque speed curve, fuel consumption and refueling infrastructure. External combustion in a steam engine seems to be a bright idea, for a cleaner and more environment friendly alternative to the IC engine that can satisfy the multiple technology requirements mentioned. One way of performing external heterogeneous combustion is to use porous ceramic media, which is a modern and innovative technique, used in many practical applications. The heterogeneous combustion inside ceramic porous media provides numerous advantages, as the ceramic, acts as a regenerator that distributes heat from the flue gases to the upstream reactants, resulting in the extended flammability limits of the reactants. The heat exchanger design is the major challenge in developing an external combustion engine because of the space, such systems consume in an automobile. The goal of the research is to develop a compact and efficient heat exchanger for the application. The proposed research uses natural gas as a fuel that is mixed with air for combustion and the generated flue gases are fed to a heat exchanger to generate superheated system for performing engine work to the vehicle. The performed research is focused on designing and modeling of the boiler heat exchanger section. The justification for selection of working fluid and power plant

technology is presented as part of the research, where the proposed system consists of an Air and Flue Gas Path and a Water and Steam Path. Models are developed for coupled thermal and fluid analysis of a heat exchanger, consisting of three sections. The first section converts water to a saturated liquid. The second portion consists of a section where water is converted to saturated steam. The third section is the superheater, where saturated steam is converted to superheated steam. The Finite Element Model is appropriately meshed and boundary conditions set up to solve the mass, momentum and energy conservation equations. The k-epsilon model is implemented to take care of turbulence. Analytical calculations following the established codes and standards are also executed to develop the design.

This work is dedicated to my friend Suhana Shabnam, who inspired me to join grad school and motivated me to keep pushing the limits of ambition and enterprise, to excel in life.

ACKNOWLEDGMENTS

My sincere thanks to Dr. Nina Orlovskaya, for her valuable guidance in this work. I would also like to thank Dr. J. Gou and Dr. Subith Vasu, for being part of the Thesis Committee. My parents, Mrs. Arundhati Dasgupta and Mr. Pranabes Dasgupta, shall be given credit for loving me and encouraging me to chase my dreams. My former colleague Ms. R. Sujatha plays a vital role in my life by always being there for me, as a friend and I take this opportunity to thank her.

I would thank all my lab mates for their help and cooperation. Special mention shall be made of Dr. Anthony C. Terracciano, my former lab mate for his valuable inputs. Samuel de Oliviera and William Henken, who worked initially as undergrad students in this project are also acknowledged.

TABLE OF CONTENTS

LIST OF FIGURES x

LIST OF TABLES xiii

CHAPTER ONE: INTRODUCTION 1

1.1. Goals 1

1.2. Alternatives to IC Engine 1

1.3. Why Steam Vehicles: Choice of working fluid 8

CHAPTER TWO: LITERATURE REVIEW 12

2.1. History of Steam Automobiles 12

2.2. Steam Generation –Technologies 15

2.3. Porous Media Combustion 19

2.3.1. Porous Materials 20

2.3.2. Excess Enthalpy Combustion 24

2.4. Applications of Porous Media Combustion Technology 25

2.5. Combustion mechanisms in Porous media burners 26

2.6. Modeling of Porous Media Combustion 30

2.7. Porous media combustion with heat exchangers 35

2.8. CFD modeling of Heat Exchangers 41

2.8.1. Flow Maldistribution 42

2.8.2. Fouling 43

2.8.3. Pressure Drop 43

2.8.4. Thermal analysis 44

2.8.5. Shell Side Heat Transfer 44

2.9. Flow in Curved Conduits 45

2.10. Heat exchangers with helically coiled tube 54

2.11. Two phase flow in a helically coiled tube heat exchanger 59

2.12. Simulation of Heat Transfer in Boilers 60

CHAPTER THREE: SYSTEM DESCRIPTION AND OVERVIEW 63

3.1. Air and Flue Gas Path 63

3.2. Water and Steam Path 66

3.3. Control Philosophy 67

3.3.1. Furnace Draft Control 67

3.3.2. Combustion Control 67

3.3.3. Control Logic 67

3.4. Combustion Chamber 68

3.5. Material Selection Philosophy 69

3.5.1. Steam Pipes: SA 106 Gr. B 69

3.5.2. External Gas Pipe: Mild Steel ERW 71

3.5.3. Boiler Heat Exchanger tubes (steam path): SS 304 71

3.5.4. Condenser tubes: SS 304 71

3.5.5. Raw water inlet pipe: SS 304 71

3.5.6. Condensate Storage Tank: PVC or SS304 71

CHAPTER FOUR: MODELING 73

4.1. Problem Description 73

4.2. Description of Software 74

4.3. Equations 75

4.4. Meshing 79

4.5. Model Geometry 84

CHAPTER FIVE: RESULTS 88

CHAPTER SIX: CONCLUSIONS 100

LIST OF REFERENCES 102

LIST OF FIGURES

Figure 1) Photograph of an Internal Combustion Engine 2

Figure 2) Photograph of a Battery Powered Vehicle 3

Figure 3)Photograph of Fuel Cell Powered Vehicle 4

Figure 4) A model of a Gas Turbine Propulsion System 6

Figure 5) Photograph of a Gas Turbine Propelled Tank 7

Figure 6) Temperature-Entropy (T-S) Diagram of R 245 fa 10

Figure 7) Photograph of Cugnot's Steam Drayss –First Steam Vehicle (1769) 12

Figure 8) Photograph of The Obedient-First Private Steam Car in Paris (1873) 13

Figure 9) Photograph of the Stanley Steam Car 14

Figure 10)Model of 150 MW Circulating Fluidized Bed Boiler 18

Figure 11) Schematic of Reaction Zone within porous media 20

Figure 12) Examples of Heat Recirculation Burners 27

Figure 13) a) Schematic representation of heat recirculation in a porous media 29

Figure 14)Schematic of Reciprocating combustion system and the profiles of Temperature T 33

Figure 15) Effect of pellet diameter D for different air flow rates, q on the peak temperature 34

Figure 16) Schematic of a porous media burner used for household heating 37

Figure 17) a) Detailed view inside the heat exchanger elements b) heat exchanger 38

Figure 18) Porous burner -heat exchanger thermal efficiency relating to LHV 40

Figure 19) Schematic Diagram of Experimental Apparatus 41

Figure 20) Axial velocity and secondary streamlines of flow within a curved conduit at various Dean Numbers. I and O denote the various Dean Numbers 47

Figure 21) Double Pipe Heat Exchanger-Coordinate System 48

Figure 22) Secondary Flow in a Helical Pipe 48

Figure 23) Annulus Nusselt Number and its variation with Dean Number 50

Figure 24) Variation of Overall Heat Transfer coefficient with Outer Dean Number 52

Figure 25) Variation of Overall Heat Transfer Coefficient with Inner Dean Number 53

Figure 26) Experimental set up for heat transfer in R134a for a helicoidal pipe 53

Figure 27) Temperature vs Flow rate for different temperatures of the helical bath for both helical and straight tubes for helical coil and straight pipe 55

Figure 28) Heat Transfer Coefficient for different conditions of the hot bath for helical coil and straight pipe 55

Figure 29) Velocity and Temperature Profile in a helical tube 59

Figure 30) Heat at different loads 61

Figure 31) CFD simulation of temperature distribution in the convection zone of a power boiler 62

Figure 32) Process Schematic 63

Figure 33)Piping and Instrumentation Diagram of Air, Fuel and Flue Gas Path 65

Figure 34) Piping and Instrument Diagram of Water and Steam Path 66

Figure 35) Visualization of Mesh Shell 3 80

Figure 36) Visualization of Mesh Shell 1 81

Figure 37) Visualization of 3 D Fluid Mesh Solid 1 82

Figure 38) Visualization of 3D mesh Solid 2 82

Figure 39) Visualization of 3D Fluid Mesh Solid 3 83

Figure 40) Visualization of straight tube heat exchanger model: tube side 84

Figure 41) Visualization of Heat Exchanger Model: Shell Side 85

Figure 42) Side View of Heat Exchanger Model 85

Figure 43) Model of Helical Coiled Tube Heat Exchanger 86

Figure 44) Section of Helical Coil Heat Exchanger 86

Figure 45) Geometric model of single tube of heat exchanger 88

Figure 46) Meshed Model of Single Tube of Heat Exchanger 90

Figure 47) Model of single tube of heat exchanger 90

Figure 48) Temperature Distribution of Steam and Flue Gas at different stages of the Heat Exchange Process 99

LIST OF TABLES

Table 1) Pore Sizes and Extinction coefficients for alumina at 488 nm 22

Table 2) Comparative data for mean diameters of web and pore for different porous materials and pores per cm specification 24

Table 3) Composition of SA 106 Gr B 69

Table 4) Composition of SS 304 72

Table 5) Design Parameters 79

Table 6) Properties of 2D Meshes 80

Table 7)Properties of 3 D extruded meshes 83

Table 8) Boundary Conditions for Simulation 89

Table 9) Average Scale Information 91

Table 10) Convergence History at Time Step1 92

Table 11) Convergence History at Time Step 17 92

Table 12) Solution Summary 94

Table 13) Result Sheet for Superheater and Economizer 96

Table 14) Results for Evaporator 98

CHAPTER ONE: INTRODUCTION

1.1. Goals

a) Design of a compact heat exchanger for steam generation, for external combustion in a vehicle
b) Develop a FEM Model for the Thermal Flow characteristics of the Heat Exchanger using Siemens NX
c) Generate Analytical Solutions and Results

1.2.Alternatives to IC Engine

The internal combustion engine **(photograph shown in Figure 1**) is highly reliable, has high power density and is easily refuel able. The technology is predominant for the last century and is the most abundant surface transport technology, even today. It is widely used for cars, trucks, and motor cycles and to a lesser extent in locomotives. However, the internal combustion engine process, is highly polluting leading to SO_X, NO_x, CO_2 and CO emissions. With issues like climate change, global warming and ozone layer depletion being the main causes of concern for the global community we are focusing on finding viable alternative technologies for vehicles.

The internal combustion engine vehicle consists of the engine, gear box, the hook's joint and the differential mechanism. The vehicle also consists of the wheel and axles and the steering mechanism. The combustion takes place in the engine, which is driven by practical realizations of the Otto cycle, Diesel Cycle or the Joule Cycle, in thermodynamics. The

combustion occurs in Four Stroke or Two Stroke cycles. A four stroke engine has four strokes-intake, compression, power (expansion) and exhaust.

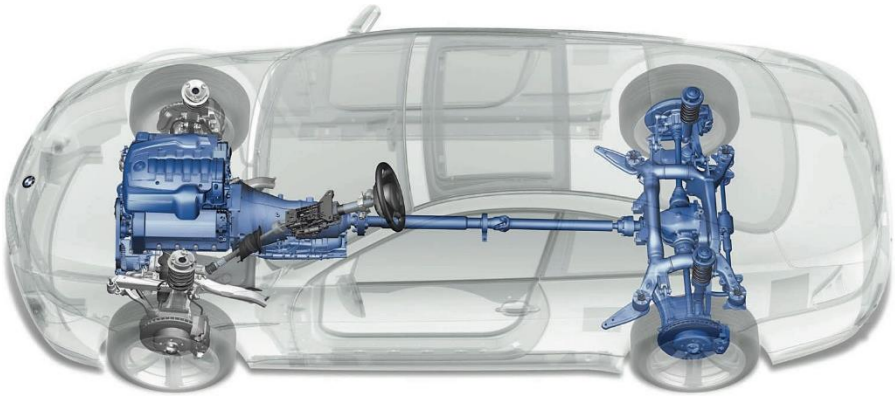

Figure 1) Photograph of an Internal Combustion Engine

The distinguishing factor of the two stroke engine is that every outward stroke of the piston is a power stroke. A two stroke engine has ports for entry and exhaust of charge. The ports are uncovered by the piston near the bottom dead center. Thus, the pumping operation is accomplished by a scavenging pump, externally. Typically the fuels used for internal[1] combustion are gasoline, diesel, and natural gas. More environment friendly fuels like bio-diesel and hydrogen are also being adopted by different manufacturers. The choice of the thermodynamic cycle for IC Engines, depends on the type of ignition system i.e. Spark Ignition or Compression Ignition.

Fuel Cells, Battery operated vehicles, hybrid vehicles, gas turbine vehicles, external combustion engines with steam working on the Rankine Cycle and Organic Rankine Cycle are some of the alternatives.

Figure 2) Photograph of a Battery Powered Vehicle

Electric vehicles have a traction motor to power the wheels. The motor may be connected to an off-vehicle power supply system like in locomotives or tram cars or be using a battery to store energy. Battery operated vehicles (**photograph shown in Figure 2**) have zero emission, high efficiency and have developed considerably over the years.[2] However they are limited by the size of the battery which makes their range lower than gasoline, diesel or gas engines[3]. Mitsubishi i MiEV, Nissan Leaf, Smart ED, Renault Fluence Z.E., Ford Focus Electric, Tesla Model S, Honda Fit EV, RAV4 EV second generation, Renault Zoe, Chevrolet Spark EV, Mercedes-Benz SLS AMG Electric Drive, Fiat 500 are some of the commercially available electric vehicles in the market, in different countries. The Plug in Electric Vehicle (PHEV) and Hybrid Electric Vehicle (HEV) are some of the types of electric vehicles available. A PHEV is any vehicle that can be charged from an external source like and stored in battery stacks. A hybrid electric vehicle (HEV) combines a conventional power train with an electric drive.

Figure 3)Photograph of Fuel Cell Powered Vehicle

Fuel Cell powered vehicles **(shown in Figure 3**) have better range than the electric vehicle and have zero emissions. But both the electric vehicle and the fuel cell vehicles are disadvantaged by high cost and limited charging/ refueling facilities.[3] Fuel cell technology has limited market penetration and are not yet technically mature. A fuel cell powered vehicle is shown in Figure 3. A fuel cell powered vehicle has a fuel cell stack to generate electricity from hydrogen gas and oxygen. The electricity drives an electric motor for propulsion. There is a battery for storing energy generated from regenerative braking and provides supplemental power to the motor and an electric Power Control Unit. Unlike an engine, a fuel cell does not burn fuel cell. The process revolves around fusion of

hydrogen and oxygen and electricity is generated as a result. Hydrogen can be stored in a tank. It can also be produced onboard the vehicle by reforming methanol, or crude oil derived hydrocarbon fuels (e.g., gasoline, diesel, or middle distillates). The vehicle design becomes simpler if direct hydrogen storage is used but it requires developing a more complex refueling infrastructure. Simulation programs of fuel cell vehicles and onboard fuel processors were developed.[4] For the same performance, hydrogen fuel cell vehicles are simpler in design, light weight, more energy efficient and of lower cost than those with onboard fuel processors.

Vehicles with onboard steam reforming of methanol or On board Partial Oxidation (POX) of gasoline have about two-thirds the fuel economy of direct hydrogen vehicles. The efficiency dips because of conversion losses in the fuel processor, losses in forming hydrogen from another fuel, performance of reformate, effects of fuel processor response time.

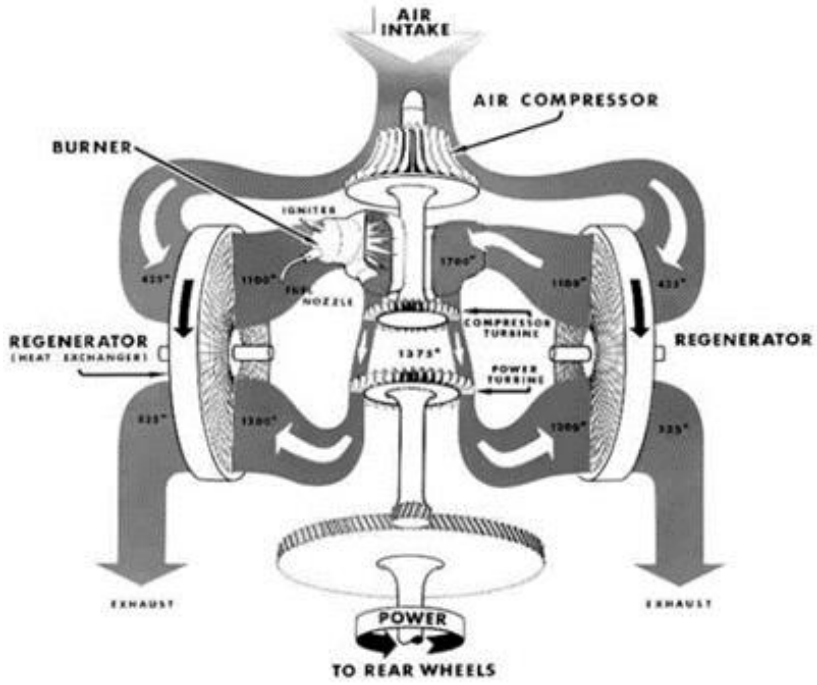

Figure 4) A model of a Gas Turbine Propulsion System

Another feasible alternative, is the gas turbine vehicle. **Figure 4 shows the model of a Gas Turbine Propulsion System**. Gas turbines are equipped with an upstream rotating compressor, a combustion chamber and a turbine mounted on the same shaft. The regenerator is a heat exchanger used to recover heat. The ideal gas turbine runs on the Brayton Cycle comprising of an isentropic compression, isobaric combustion and an isentropic expansion. Gas turbines are often used in ships, locomotives, helicopters, tank propulsion. They are used to a lesser extent in cars and motor cycles. The gas turbine is less polluting and more efficient than the IC Engine. Some of the advantages are, long life due to no rubbing parts like pistons, absence of large vibrational forces due to reciprocating components, which even with balanced crank configuration necessitates heavy internal

construction, low lube consumption, and no cooling water.[5] But it is not possible to use them due to the high manufacturing costs, especially at lower capacities and the poor throttle response. Another drawback of the gas turbine is high off-design fuel consumption. Unlike power stations, automobile power plants have to operate at off design conditions, due to continuously fluctuating load.[6] A well-known limitation of the turbine vehicle is the delay in acceleration from rest while the gas-generator unit is speeding up.[5]

Figure 5) Photograph of a Gas Turbine Propelled Tank

Figure 5 shows the photograph of a military tank propelled by a Gas Turbine. Starting in mid-1944, the German Army's development division, the Heereswaffenamt (Army Ordnance Board), studied several gas turbine engines for use in tanks. The first gas turbine engine, was installed in the Panther tank, for armored fighting vehicle GT 101 . In 1954, there was the second use of a gas turbine in an armored fighting vehicle, when a unit, PU2979, developed by C. A. Parsons & Co., was installed in a British Conqueror tank. The Stridsvagn 103 was developed in the 1950 s. It was the first mass-production main battle tank using a gas turbine engine. Since then, gas turbine engines have been used

as Alternate Power Units (APU) in many tanks .They have also been used as main power plants in Soviet/Russian T-80s, U.S. M1 Abrams tanks, among others. As compared to https://en.wikipedia.org/wiki/Diesel_engine tanks they are lighter and smaller, at the same sustained power output but are less fuel efficient than the equivalent diesel, at idle. At idle they require more fuel to achieve the same combat range. This problem has been, addressed with battery packs or secondary generators to power the tank's systems while stationary. This strategy saves fuel by reducing the need to idle the main turbine. T-80s have the capability to mount three large external fuel drums which can greatly extend their range. Russia stopped production of the T-80 and phased it out with the diesel-powered T-90. Ukraine uses the diesel-powered T-80 UD and T-84 with nearly the same power of the gas-turbine tank. The French Leclerc MBT, uses the "Hyperbar" hybrid supercharging system. In this system, the engine's turbocharger is replaced with a small gas turbine which is an assisted diesel exhaust turbocharger thereby enabling engine RPM-independent boost level control and a higher peak boost pressure to be reached (than with ordinary turbochargers). This system enables a smaller displacement and lighter engine and effectively removes turbo lag. This turbocharger can also function, independently from the main engine as an ordinary APU.

1.3.Why Steam Vehicles: Choice of working fluid

The disadvantages of developing technologies like Fuel Cells and Battery makes us shift our focus to External combustion technologies. External combustion is less polluting than the IC engine. Also unlike fuel cell and batteries, we can use conventional fuels like natural gas, methane or diesel or kerosene thus necessitating no change to the fuel distribution

networks available. These engines can be designed for multi-fuel capability, have simple idling procedure and a favorable torque speed curve. There are two potential candidates for the working fluid for an External Combustion engine for vehicles –steam and organic fluids (using Organic Rankine Cycle).

Organic Rankine Cycles (ORCs) have been developed for use in medium scale CHP systems (> 500 kW), but have some drawbacks. ORC research is showing a fast growth However, most of the recent studies deal with theoretical aspects. Information on the practical usage of the ORC is limited. ORCs can use scroll and screw expanders instead of turbines and engines. Both expanders have significant potential to produce power from low-grade energy[7].

Fluid selection for the Organic Rankine Cycle is a critical issue and is dependent on the target application, on the working conditions and even on the criteria considered.

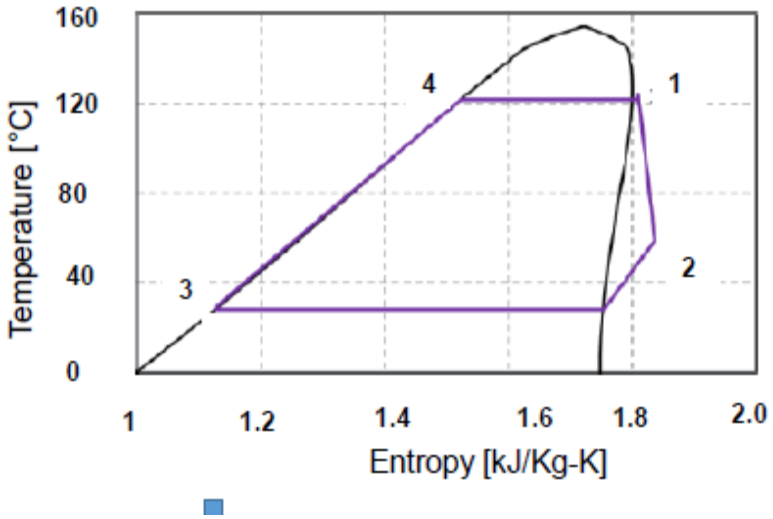

Figure 6) Temperature-Entropy (T-S) Diagram of R 245 fa

ORCs offer a solution to the replacement of conventional technologies, at the expense of high fluid flow rates and large condenser size. Water Steam Cycles, offer higher pressure ratios, which can be obtained with modern heat exchangers and condensers of small area. Water has better heat-transfer characteristics than organic fluids. The shortcomings of water such as freezing and air infiltration can be minimized and water is the most practical working medium for thermal recovery cycles ahead of Organic fluids. Organic Fluids have much lower efficiency as compared to water in a Rankine Cycle. The different organic fluids used and ranked from the highest to lowest order of efficiency are n-butane, R245fa, R123, n-pentane, HFE7000, SES36, R134a, R1234yf.[8] and even the most efficient is less than 10 % efficient. **A T-S Diagram for R245 fa, for Organic Rankine Cycle is shown in Figure 6.** Even the maximum temperature achieved in the cycle is as low as 160 ºC, which severely undermines power generated. Thus, in keeping with the small surface area

and high efficiency required for our design, steam is the most viable option for external combustion ahead of organic fluids.

CHAPTER TWO: LITERATURE REVIEW

2.1.History of Steam Automobiles

Steam-engines have an exceptional place in automotive history. The first self-propelled vehicle, *Fardier à vapeur* (translation: *Steam Dray*), was a steam-engine design by French engineer Nicolas Cugnot [9, 10]built in order to move French artillery pieces. **Figure 7. shows Cugnot's *Steam Dray*, built in 1769**. This car preceded Karl Benz's internal combustion engine design by over a century. In 1770, a full-size version of the *fardier à vapeur* was developed, and declared to be able to carry 4 tons and cover 2 *lieues* (7.8 km or 4.8 miles) in an hour. This performance was never achieved in practice.

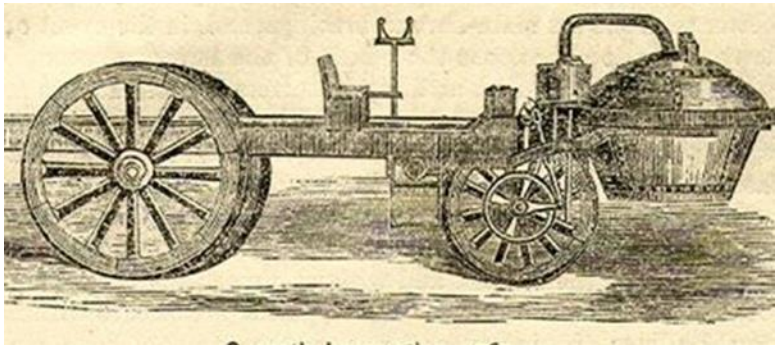

Figure 7) Photograph of Cugnot's Steam Drayss –First Steam Vehicle (1769)

The vehicle, which weighed about 2.5 tons, had two wheels at the rear and one in the front where the horses would normally have been; this front wheel supported the steam boiler and driving mechanism. The power unit was articulated to the "trailer" and steered from there by means of a double handle arrangement This 8000-pound vehicle had a tricycle design with two wheels in the back and one steerable front wheel, which was also the drive wheel. Plagued by weight-distribution and steam-pressure issues, as well as a poor boiler

design, it was subsequently abandoned as a futile method of locomotion by the French army. Nonetheless, Cugnot's *Steam Drayss* was capable of carrying 4 passengers at speeds of 2-3 miles per hour, effectively making it the first automobile, and thus proving the feasibility of steam-engine designs for automobiles. [11]

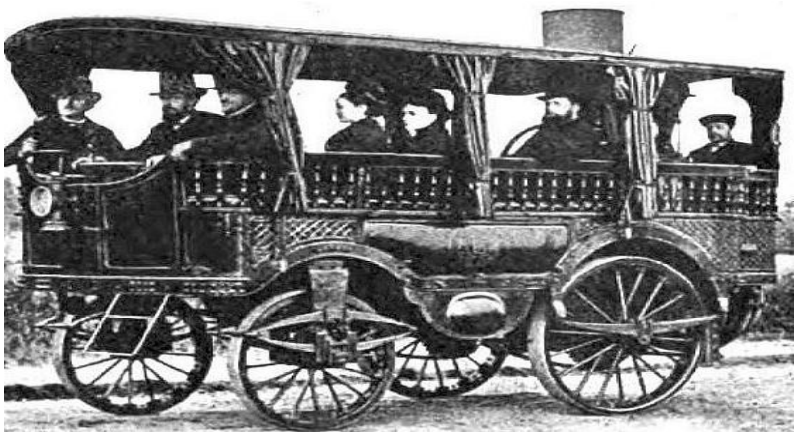

Figure 8) Photograph of The Obedient-First Private Steam Car in Paris (1873)

The use of steam engines in automobiles was hampered by the enormous size and weight required in early designs, so most of the innovation in steam-engine design was geared for steam-boats and locomotives. Still, there was progress with the steam-car. 1873 saw the introduction of *The Obedient*, by French bell-maker Amédée Bollée. **This steam car, shown in Figure 8** could carry up to a dozen passengers, achieving speeds of 19 miles per hour. This is the first vehicle that showed satisfactory performance by its speed and maneuverability. It is regarded as the ancestor of the modern automobile. It weighed 4800 kg. Two years later, it would make the 130-mile trip from Le Mans to Paris in 18 hours. Although there was fierce competition between the steam-engine and the internal-combustion engine, steam-engines still had the edge in performance and market-share. It

was propelled by two units of V-twin steam engines, one used for each rear wheel. The original vehicle can still be seen in the collection of the Conservatoire National des Arts et Métiers in Paris. Indeed it was the first private automobile vehicle allowed to travel in the roads of Paris.[10]

At the turn of the century, steam-cars were more than half of all vehicles on the road in America. The zenith of steam-car design came with the introduction of the Stanley Steamer, a variant of which would set the land speed record in 1906, with a confirmed top speed of 128 miles per hour. [11]Steam-engines eventually fell out of favor, as the internal combustion engine improved, making it a more appealing option due to its convenience and lower cost. **Figure 9 shows the photograph of the Stanley Steamer**.

Figure 9) Photograph of the Stanley Steam Car

Perhaps the most famous and best-selling steam car was the Stanley Steamer, manufactured commercially from 1896 to 1924. In the period between 1899 and 1905, Stanley outsold every gasoline-powered car, and was second in sales only to the electric cars of

the Columbia Automobile Company in the US. Stanley a compact fire-tube boiler, to power a double-acting two-cylinder engine. Due to the huge torque available at all ranges engine speed, the engine was geared directly to the rear axle, without any clutch or variable speed transmission. Until 1914, Stanley steam cars rejected exhaust steam directly to the atmosphere. This necessitated refilling of the water tank after 1914. The inclusion of a condenser, considerably reduced the water consumption.

In 1906 Fred Marriott piloted a Stanley car, at 127 mph (204 km/h) at Ormond Beach, Florida. This was the land speed record and was not exceeded by any car until 1910.

In recent years, there has been a reinvigorated interest in the steam-car, fueled by concerns about the need for vehicles emitting fewer pollutants. In 2009, a student project from Southampton University led to the construction of a steam car, the *Inspiration*, which managed to beat the steam-car land-speed record, with a speed of 140 miles per hour. Steam-engines, given their ability to operate on different fuels, could also address concerns about dependence on non-renewable petroleum-derived fuels. Many of the issues extant in early steam-engines and power plant designs, like cold-start wait time and pressure loss, have been remedied with modern engineering and technology, making steam-cars a candidate for future passenger vehicles.

2.2.Steam Generation –Technologies

Steam can be generated by conventional methods like combustion of fossil fuel like coal and natural gas through a Rankine Cycle using Steam Turbines or Reciprocating Engines.

It can also be generated by Solar Thermal Technology or by the combustion of Nuclear Fuel. In areas with appropriate resources geothermal technology may be used for generation of steam.

Nuclear power technology uses uranium, thorium and other radioactive materials to execute nuclear reactions that generate steam in a Nuclear Reactor. The reactions include nuclear fission, nuclear fusion and decay. The International Generation –IV initiative aims at fostering research and development of new generation nuclear systems.[12] The systems identified for next generation technology improvement are:

- Very High Temperature Gas Cooled Reactor
- Gas Cooled Fast Reactor
- Sodium Cooled Fast Reactor
- Lead Cooled Fast Reactor
- Molten Salt Reactor

Solar Thermal plants use solar energy to replace fossil fuels for steam generation in a boiler. Three types of solar thermal plants for steam generation are common-parabolic troughs, dishes and the central receiver with heliostat fields. Parabolic troughs are most popular. In such systems, the transfer medium is organic oil for temperatures of 300°C or expensive synthetic oil for temperatures up to 400°C. The power conversion uses one or two heat exchangers to obtain saturated or superheated steam. There is a system to convert the thermal energy and the waste heat is rejected. A more advance system is an Integrated Solar

Combined Cycle System (ISCCS). This is a hybrid system with a gas fired turbine and a solar field. Solar field with parabolic trough can generate steam and this steam can be sent to a fossil superheater to work like the conventional coal fired power plant. Another interesting approach is direct steam generation (DSG) with parabolic trough. DSG eliminates oils as well as heat exchangers. The transfer fluid temperature is elevated.[13]
Conventional Coal Fired Systems use Fire Tube as well Water Tube Technologies. Coal fired boilers are conventionally of the Pulverized Fuel (PF) type. Another technology which is fast replacing the PF boilers, is the fluidized bed technology.

Numerical CFD modeling of a 150 MW Circulating Fluidized Bed Boiler (CFBC) was performed[14].**Figure 10 shows the model of a CFBC boiler with its full geometry**. At the bottom of the boiler furnace there is a bed of inert material. The bed is where the coal or fuel spreads. Air supply is from below the bed at high pressure. This lifts the bed material and the coal particles and keeps them in suspension. The coal combustion takes place in this suspended state. This is the Fluidized bed and is the defining feature of this technology. Fine particles of partially burned coal, ash and bed material are circulated along with the flue gases to the upper part of the furnace and then into a cyclone. The heavier particles separate from the gas and falls to the hopper of the cyclone and are returned to the furnace for recirculation. Hence the name Circulating Fluidized Bed combustion. The hot gases from the cyclone pass to the heat transfer surfaces and go out of the boiler. Special design of the air nozzles at the bottom of the bed allows flow of air without clogging. Primary air fans provide preheated Fluidizing air.

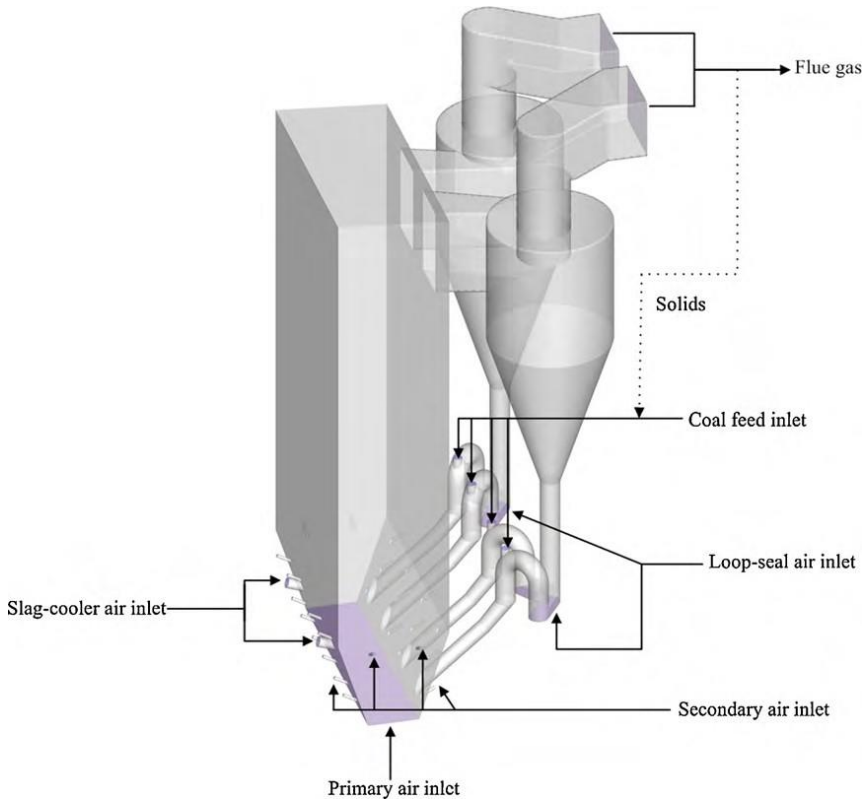

Figure 10)Model of 150 MW Circulating Fluidized Bed Boiler

Secondary air fans provide pre-heated Combustion air. Nozzles in the furnace walls at various levels distribute the Combustion air in the furnace Due to low emission and fuel economy CFBC is a very sophisticated boiler technology for steam generation. The figure below shows the geometry of a 150 MW steam generator. The significance of this simulation was unlike most other works, it was not limited to the combustion chamber but encompassed the full loop. The pressure gradient is large at the bottom and small at the top. The phase coupled SIMPLE algorithm was chosen for pressure-velocity coupling in the model. The vertical velocity of the solids in the boiler was positive in the center and negative near the wall.

2.3.Porous Media Combustion

For steam generation, a combustion process is required. One of the combustion processes that is gaining a lot of attention is combustion in porous media. Porous media combustion, is an exothermic reaction during flow of fluid in a porous medium (PM) packed bed. This method of combustion gives rise to high radiant output, low NOx and CO emissions, high flame speed and higher power density. A porous material has connected voids which the flow can penetrate. The combustion efficiency of PM burner is higher and there is a better heat transfer from burned gases to unburned mixture compared to conventional burning. PM combustors have better homogenization of temperature across the PM and a fair amount of radiation helps to preheat the incoming air-fuel mixture. This technique has been used for gaseous and liquid fuels in both steady and unsteady combustion. Pre-mixed combustion is a very effective way to enhance combustion by porous media. Steady state combustion is widely used in radiant burners and surface combustor-heaters due to the high radiant emissivity of the solid. The combustion zone is stabilized by the solid. The other way to go about PM combustion is transient combustion which leads to an unsteady reaction zone that freely propagates as a filtration combustion wave in the downstream direction. Combustion in PM differs considerably from the homogeneous flame front. Important features of PM for application of combustion technology are: large specific surface area, excellent heat transfer properties, heat capacity, transparency for fluid flow, thermal resistance, mechanical resistance, recuperation of energy and electrical properties **[**15].**Figure 11 shows a schematic of the reaction zone within porous media.**

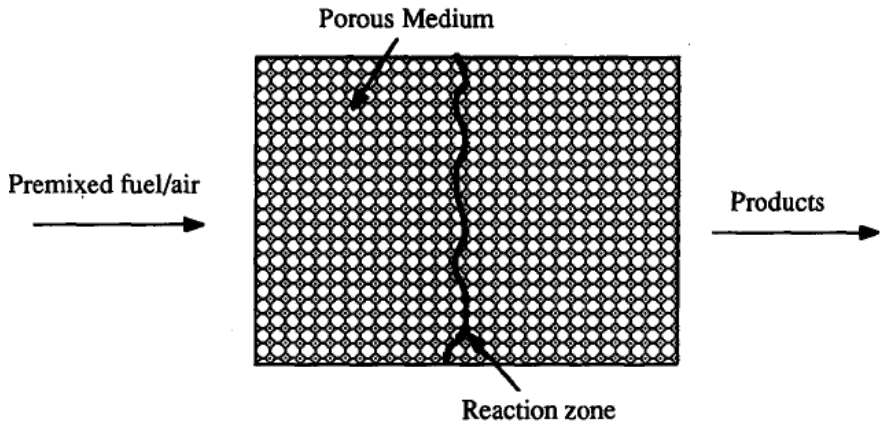

Figure 11) Schematic of Reaction Zone within porous media

2.3.1. Porous Materials

The choice of material for porous media burners can be tricky. Combustion temperatures of PM burners can be designed to be relatively low by lean burning. Still, those lower temperatures are sufficient to allow quick degradation of the fine structure of those materials. So, ceramics are suitable for this application to avoid degradation. Availability of porous ceramic foams and discrete ceramic matrices are important advances. While porous ceramic foams have good temperature resistance their durability does suffer from differential stresses suffered from expansion at different temperatures. Reticulated porous ceramic foams typically have an open pore structure with a dodecahedral geometry.

a. Porous Ceramic Foams

The porous matrix structure is specified by the mean pore size and the porosity. The porosity is typically about 85%. Available pore sizes range from approximately 25 to 2 pores per centimeter (pack) or 65 to 8 pores per inch (ppi).

The ceramic foams can have a variety of compositions. They usually have a base material like silicon carbide, silicon nitride, mullite, cordierite, alumina, and zirconia. There is also a binding material to stabilize like magnesium or Ytrium. Orenstein and Green investigated the thermal shock behavior of alumina -mullite ceramic foam material. The specimens were immersed in oil and water. The pre-quench temperature was 1500°C. immersed specimens at pre-quench temperatures of 1500°C, to investigate the thermal shock of alumina-mullite ceramic foams. It was found that the thermal shock increases with pore size and the dependence is strong. The damage was caused by a temperature expansion, across the bulk and not individual struts of the porous material.

Hsu and Howell measured the effective thermal conductivity (k) for samples of Partially stabilized zirconia (PSZ) (zirconium oxide plus < 3% magnesium oxide) of pores ranging from 4 to 26 ppcm in size. From experiments the following correlation was developed for the temperature range 290K-800 K and for pore diameters between 0.3 and 1.5 mm.

$k\ [W/(m.\ K)] = 0.188 - 0.0175d$

where d is the actual mean pore diameter (mm).

The correlation was developed by measuring the thermal conductivity by a guarded hot plate method. Corrections for radiative transfer through the porous material were done using a two-flux method. It was seen that the thermal conductivity is negligibly effected by temperature. At low temperatures, pure zirconia has a stable monoclinic structure. However, between temperatures 1100°C and 2283°C, pure zirconia undergoes phase transitions to a cubic solid structure. To suppress such phase transitions MgO is added to PSZ. Despite these additions, some transition is detected in burner applications of PSZ.

Hsu and Howell, [15] developed the correlation, is $T = 1340 - 1540d + 527d^2$ where T- is the mean (spectrally averaged for long wavelength radiation) extinction coefficient and d is the actual pore diameter in mm, for pore sizes $0.3mm < d < 1.5mm$ and for temperatures, $290 < T < 890$ K. On the basis of a two-flux radiation model for measuring the extinction coefficient and using geometric optics for predicting properties the following correlation is developed between the radius and the pore size:

$$r = \left(\frac{3}{d}\right).(1 - p) \quad (1)$$

Isotropic scattering, is a necessary assumption for the techniques used for developing the correlations. Hence, independent values of albedo, scattering or absorption coefficients cannot be determined**. Table 1 shows the calculated extinction coefficients by Hsu and Howell**[15]

Table 1) Pore Sizes and Extinction coefficients for alumina at 488 nm

Parameter	**Value**			
Pores (ppcm)	4	8	12	26
Extinction coefficient (m^{-1})	1000 ± 100	1150 ± 50	1200 ± 100	2500 ± 100

b. Porous Media of Discrete Elements

The previous section discusses porous media as ceramic foam. Porous medium can also be formed from discrete element bed and used for burners and reactors. This type of elements does not have a rigid matrix, which makes them durable and robust. A ceramic matrix of

saddles or balls is used to manufacture reactors from porous discrete element reactors. The typical porosity of a packed bed of spheres is in the range of 0.36- 0.43.

Higher porosity is due to the irregular geometry of the saddles. **Table 2 lists comparative data for different porous materials, including, mean web diameter, mean pore diameter and parts per cm**.(ppcm).

Table 2) Comparative data for mean diameters of web and pore for different porous materials and pores per cm specification

ppcm	**Alumina**	**Cordierite**	**Partially stabilized Zirconia**	**Partially stabilized Zirconia**	**Partially stabilized Zirconia**	**Silicon carbide**	**Silicon carbide**
	Mean pore diameter mm	Mean pore diameter mm	Mean pore diameter (mm)	Mean pore diameter (mm)	Mean web Diameter (mm)	Mean pore diameter mm	Mean web diameter mm
4	1.52		1.450	1.346	0.506	1.725	0.686
8	0.94	1.25	0.967	0.737	0.356	1.015	0.508
12	0.76		0.708	0.610	0.254	0.800	0.279
18	0.42		0.467	0.467	' 0.150		
26	0.29		0.335	0.335	0.75		

2.3.2. Excess Enthalpy Combustion

In porous media combustion, the lean flammability limit can be increased and higher effective flame speeds can be achieved than the laminar flame speeds of the reactants. This is enabled by internal recirculation of heat from the downstream product

gases to the upstream reactant gases. According to Weinberg energy can be' borrowed' from a premixed flame to preheat and increase the enthalpy of the reactant gases, which are yet to burn. Thus, theoretically the peak temperature can exceed the adiabatic flame temperature locally. However, the exit temperature from the burner can never be higher than the adiabatic flame temperature, so that the first law of thermodynamics is not violated.

Excess enthalpy combustion can result in flames with higher limit than a conventional flame, thus in theory crossing the adiabatic flame temperature at its peak. An experiment with a fused silica burner and a heat exchanger demonstrated that CO emissions go down, with leaner reactant mix. It also has an indirect effect of reducing global temperatures and thus reducing generation of NO. [15]

2.4.Applications of Porous Media Combustion Technology

M.A. Mujeebu et. al. [16] reviewed the applications of porous media combustion technology. This technology has applications for IC Engines, gas turbines and propulsion, oil and gas recovery, heat exchangers, lighting, hydrogen production, Volatile Organic Components Synthesis etc. A porous burner with matrix stabilized combustion for gas turbines was built by Elzey and William Jr. A numerical model for evaporation in porous media for gas turbine has been developed by Periaswamy et. al. Evaporation of a point wise injected kerosene spray in a carbon-carbon porous medium was considered in light of the effects of porous medium temperature, fuel flow rate, air inlet temperature and porous medium geometry was conducted. It was observed that evaporation characteristics did not

vary much with porous medium geometry. The porous medium was modeled as a momentum sink. In the context of propulsion and surface transport the characteristics of porous medium which are relevant are the ability to burn learner and hotter than a free flame with low emissions, no cooling requirement for combustor and noise-free operation of the combustor. Delalic et al.[17] conducted experiments with porous medium burners built in heat exchangers for boilers, for increasing the efficiency with decreased emissions. Malico et .al[18] predicted numerically the temperature profiles and pollutant formation in a porous burner .The burner mentioned comprised of a heat exchanger for household water heating. Park and Kaviany studied thermal regeneration for diesel engines for the role of porous insert motion and the fuel injection strategies, on the fuel evaporation and combustion. The porous insert is attached to a rod and moves in the cylinder, synchronized but out of phase with the piston. During regenerative heating stage, the regenerator remains just below the cylinder head for most of the period. During regenerative cooling stroke the regenerator moves up and remains in the original position until the next regeneration heat stroke.

2.5.Combustion mechanisms in Porous media burners

Progress in Energy and Combustion Science, 2008. **34**(5): p. 667-684 Wood et al.[19] reviewed porous burners for lean applications. Porous burners are an important possibility for combusting lean fuels which are usually not flammable in conventional burners. The porous matrix serves as a means of recirculating heat from the hot combustion products to

the incoming reactants, resulting in higher flame speeds and extended flammability limits. The review is particularly focused on ultra-lean combustion, where the concentration of methane is below 5 % by volume of air.

For a laminar premixed flame the adiabatic flame temperature is defined as the theoretical temperature obtained, if all the heat released is used to raise the temperature of the products of combustion. This is solely a function of the composition of the reactants and the fuel /air ratio. Excess enthalpy burning is a process where the enthalpy of the products of combustion is added to the reactants to pre-heat them.[19] This leads to flame temperatures and burning velocities greater than the adiabatic flame temperature and is commonly referred to as superadiabatic combustion.

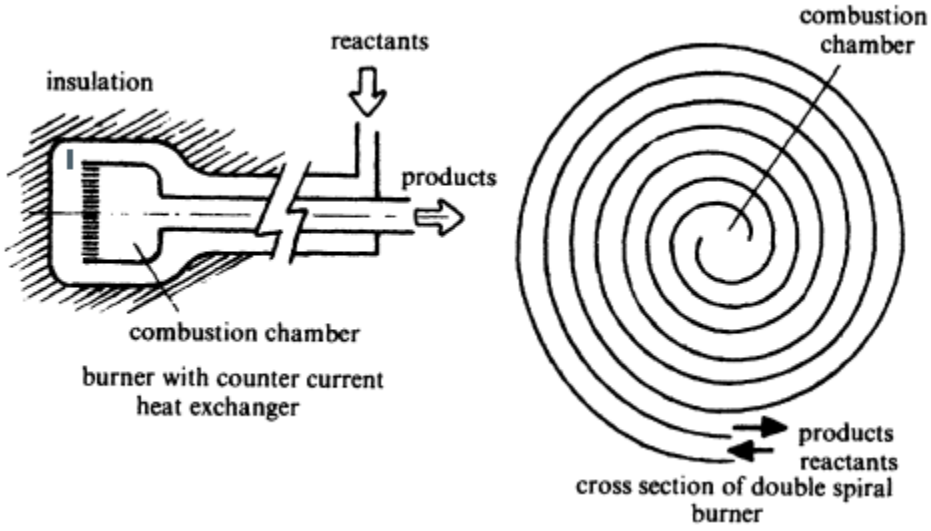

Figure 12) Examples of Heat Recirculation Burners

An alternative way of achieving excess enthalpy combustion is to insert a porous solid with better heat transfer properties into the combustion zone. Thus, the heat is recirculated internally. Takeno and Sato et. al could demonstrate experimentally that higher flow velocities can be sustained for combustion than what is attributed to the externally preheated gases alone due to the contribution of internal heat recirculation provided by the porous solid. This was done in a combustion chamber with a porous media and an arrangement of heat exchanger tubes surrounding it. **Figure 12 shows examples of heat recirculation burners.**

Heat recirculation in a porous media involves all three modes-conduction, convection and radiation. **Figure 13 illustrates the heat transfer mechanism.** Downstream of the reaction zone, the gas is hotter than the solid and thus convectively transfers heat from the products of combustion to the porous matrix. The hot solid conducts and radiates heat in the upstream direction. In the upstream reaction zone the temperature of the solid exceeds the gas and there is a heat transfer by convection from the porous matrix to the incoming gases.

To stabilize the combustion in the porous medium it must be ensured that the fame speed is equal to the incoming velocity. When the flow velocity is greater than the flame speed, the flame speed is propagated downstream and vice-versa. A decrease in fuel concentration is expected to increase flame speed. The flame shall move to a new downstream location for the flame speed to increase to match the flow velocity again. A combustion process

thus would be stable in flow and concentration. If the flow increases instantaneously the flame will move downstream –the resulting increase in pre-heating will increase the flame speed and return it to its original position.

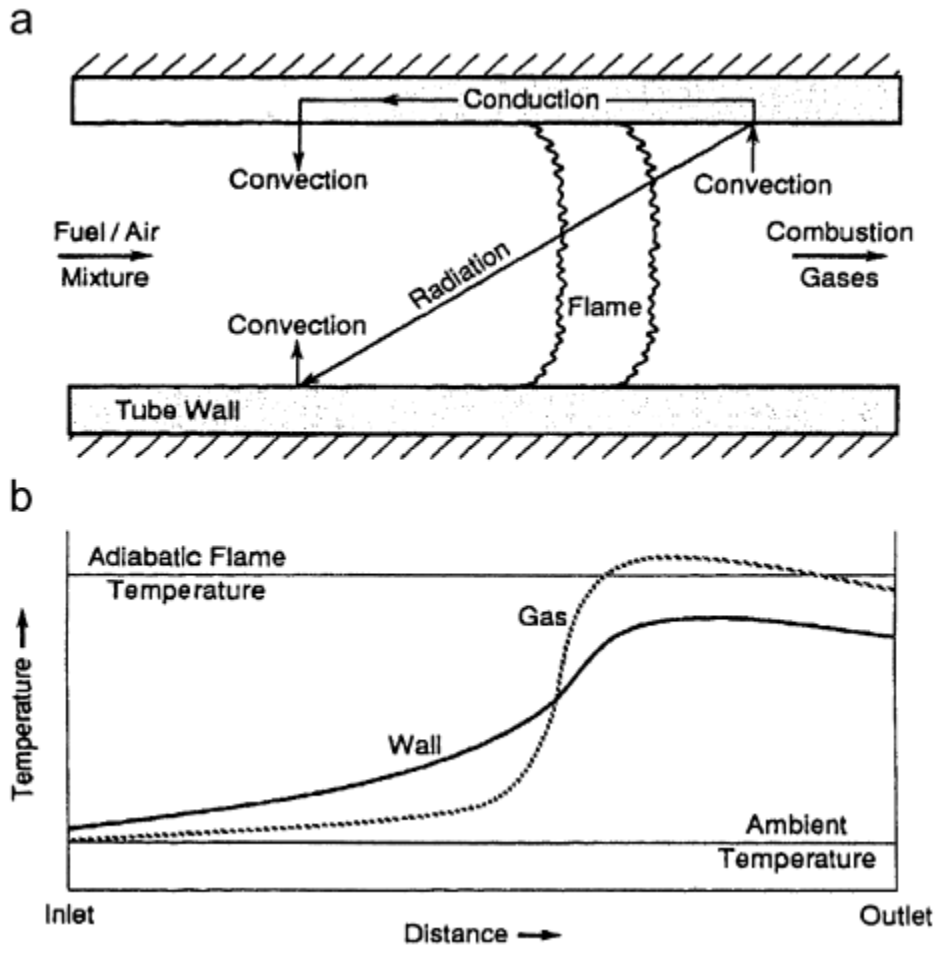

Figure 13) a) Schematic representation of heat recirculation in a porous media
b) Corresponding variation in gas and tube wall temperature with distance

Where the energy content of the fuel is extremely low, transient conduction may be used. The transient regime transfers heat more effectively than a more stabilized flame. Most studies report a vertical cylindrical structure for a porous burner, with the reactants entering

the zone from below and passing through the porous bed upwards. For radiant burners, square or rectangular cross-sections are more common. Axial flow is commonly used for porous burners. But studies done with cylindrical or spherical geometries where the flow is in the radial flow direction show that because the flow velocities are inversely proportional to radial location they provide a means of stabilization of the flame.

2.6.Modeling of Porous Media Combustion

For predicting the combustion characteristics of porous media, numerical modelling techniques have been extensively used. A numerical study through computational simulation combustion of an ethanol/air mixture in porous media burners was performed in Ansys Fluent.[20]. The Investigation was a comparison between a standard one directional flow reactor (SISO) and a reciprocal flow burner (RFB), for filtration velocities u_g=0.1, 0.3.0.5 m/s, to obtain the minimum equivalence ratio $\emptyset\ min$. Analysis of the results for the SISO reactor showed that the use of alumina balls was more advantageous compared to alumina foam for leaner mixtures over a wide range of gas velocity. It was observed that increasing the gas filtration rate, the minimum valves of equivalence ratio decreased, from 0.054 to 0.050 for alumina foam and from 0.048 to 0.044 for alumina sphere's case. The combustion front velocity goes higher for increasing filtration velocity of the mixture. The front velocity decreases with increasing fuel composition. For the same condition, the temperature inside the reactor with alumina spheres are greater than alumina foam. The combustion front velocity is lower with alumina spheres.

However, a reactor constituted by a single porous medium has a time limit in terms of its operation: as the flame is always moving, when it reaches one of the two ends of the incinerator it is extinguished.

A method of limiting the combustion front inside the porous medium is the use of RFB. RFBs operates under a periodic replacement of the gas flow direction and thus the combustion front at the center of the incinerator. Alumina balls were more efficient in terms of flame confinement within the incinerator. They exhibited, no major changes the temperature profile during 8750 [seconds] of simulation. However, alumina foam does not sustain the combustion front at the center of the burner, and the maximum temperatures tends towards the ends of the incinerator, bringing instability to the operation.

Hoffman et. al reported experimental results on the behavior of reciprocating superadiabatic combustion system, the attainable flammable limits and the low NO_x, CO emissions which can be achieved with this system. Flow velocity, half cycle, equivalence ratio and their effect on the development of temperature profiles in a porous body was studied. [21].The experimental set up consisted of fresh premixed combustible gas introduced alternatively from both sides of the porous medium at a constant velocity. The flow direction is reversed alternately. The incoming gas enters the system at ambient temperature and is preheated by the porous medium to a temperature, where reaction occurs. **A schematic of the experimental set up is shown in Figure 14.** The combustion chamber consists of a central test section, insulation and an outer housing. The section is

made of 0.1 mm stainless steel foil with a length of 480 mm and a cross section of 115 x 115 mm^2. The porous medium with a cross-section of 100 x 100 mm^2, is tightly wrapped into ceramic fiber, leaving only the inlet and outlet areas open. The outside of the test section is also insulated by 92 mm ceramic fiber board. The insulation is sufficient to keep the heat losses to the side walls below 9 % of the total heat input, even under the most adverse conditions. To ensure nearly. Three different porous media, with a porosity of 87.5 % for used. The difference was mainly in the pore size (6, 13 and 30 pores per inch respectively). The different pore sizes lead to different absorption coefficients and different effective internal volumetric surface areas for convective heat transfer between the porous medium and the fluid. The porous media is preheated by combustion of high calorific fuel gases. The porous medium has a gap of approximately 1.5 cm at the central cross-section to initiate ignition, by spark. Once stabilized combustion is achieved the spark is removed and equivalence ratio is gradually increased.

Results: It was observed that that with fine porous media the combustible limit was extended to an equivalence ratio, $\varphi = 0.026$.However deteriorating performance was observed for very coarse medium.CO emissions were observed to be strongly influenced by the porous medium used. Coarse medium showed better results. To combine the favorable effects of fine porous medium on thermal structure with low emission values obtained with coarse porous medium, a combination of both materials with the coarse media placed in the reaction zone and fine medium towards the upstream and downstream ends was proposed to achieve cleaner high performance, with extended flammable limit.

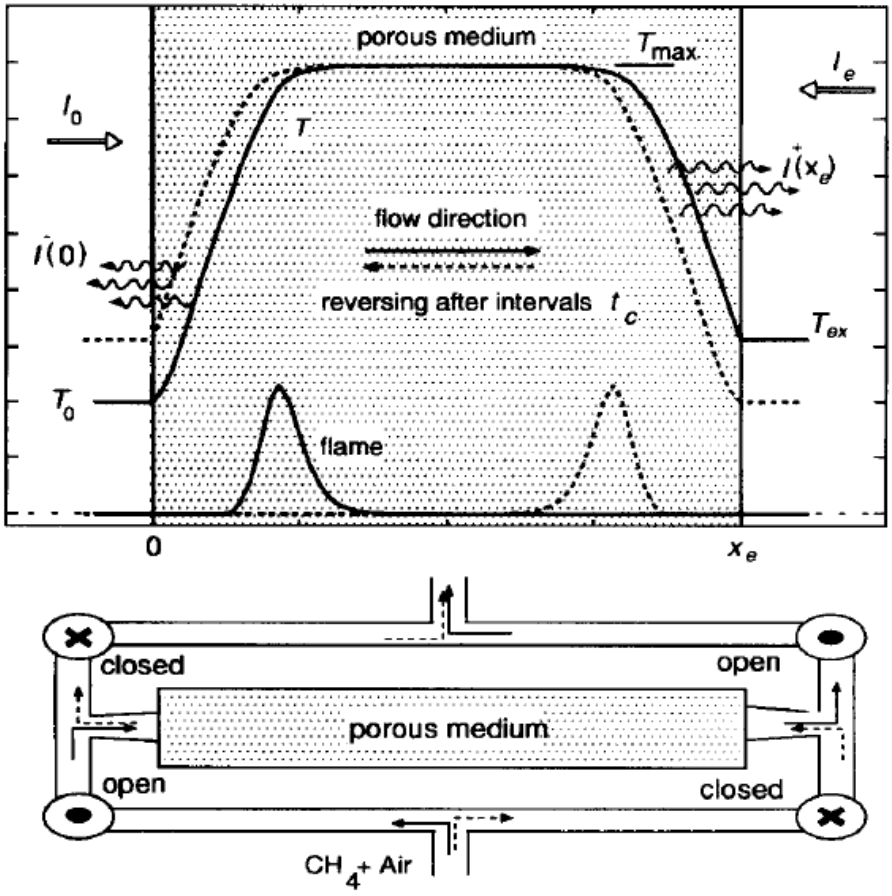

Figure 14)Schematic of Reciprocating combustion system and the profiles of Temperature T

Stationary and transient combustion zone systems are the two major approaches for design of combustion in porous media. The stationary approach is used where the combustion zone is stabilized within the porous matrix, as in radiant burners and surface combustor heaters. The transient approach is about an unsteady combustion zone which propagates as a wave either in the downstream or upstream direction, thereby adding or subtracting enthalpy fluxes, which make the combustion temperatures significantly different from the adiabatic flame temperature.

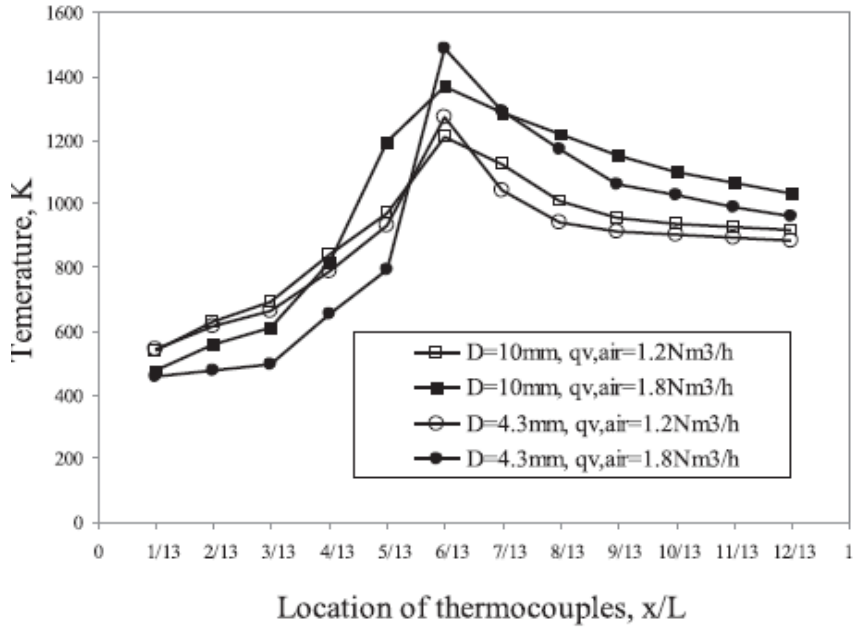

Figure 15) Effect of pellet diameter D for different air flow rates, q on the peak temperature

A porous media burner of tubular construction and filled with aluminum pellets of diameters 10 mm and 4.3 mm respectively, was used for combusting with premixed methane and air. The effect of equivalence ratio, burner inlet flow rate and diameter of pellets on the combustion temperature distribution along the burner axis and the combustion wave velocity are reported in this paper. The results proved that superadiabatic combustion can be achieved for combustion wave velocity greater than zero.[22] The critical equivalence ratio corresponding to the superadiabatic combustion was bigger for the smaller pellet diameter or higher inlet flow rate. The detailed temperature variation during start up and switch off processes of the porous media burner, was measured and

analyzed. The results showed, the temperature decreased at preheating zone and increased at the reaction zone and post reaction zone with increased air flow rate from 1.2 Nm^3 to 1.8 Nm^3 and increased equivalence ratio from 0.25 to 0.4, The peak temperature increased at the preheating and post reaction zone and decreased at the reaction zone, with the increase of diameter of aluminum pellets from 4.3 mm to 10 mm. **Figure 15** shows the variation of temperature along with the location of thermocouples for different air flow rates.

2.7.Porous media combustion with heat exchangers

The heat generated in a porous media combustion is carried by flue gases. The heat can be recovered and transferred to water/ steam in a heat exchanger. Several studies with a heat exchanger coupled to a porous media combustor have been reported in literature.

Avdic et. al. [23] developed a small scale porous media combustion system connected to a heat exchanger for space and domestic work heating. The schematic of the process is shown in **Figure 16. Figure 17** provides a detailed view of the heat exchanger elements. Experimental work was carried out on the Porous Media Burners to analyze the temperature distribution of exhaust gases close to the outer surface of a ceramic matrix and to establish the pollutant emissions as a function of burner power and air ratio number. The temperature. Conventional, open flame gas burners have low dynamic range, i.e. low power modulation capability, compared to porous media, at part load and, additionally, have higher production of carbon monoxide (CO) and nitrogen oxides (NOx). This is notable when the burner operates at low thermal power ranges. The schematics of the burner is

shown in the figure below. The region C is made up of porous ceramic Alumina fiber way lamellae structure, with porosity of 0.95. Region A is made up of Zirconia foam. Alumina is thermally stable and exhibits moderate thermal resistance to thermal shock. The air-fuel mixture is delivered by a blower, coupled with a proportioning nozzle. The porous burner is integrated with the blower. The thermal power of the system was regulated by a controller software which governed the fan speed and fuel pressure. A mobile IM 3000 P gas analyzer was used for monitoring the exhaust emissions. The thermal power of the burner was estimated using a gas flow meter. The experiment was conducted in steady state and the thermal power of the porous matrix burner was varied between 6.4 to 1.43 kW. A heat exchanger was developed for exhaust gas to water heat exchanger, consisting of two coupled components, a classical finned tube heat exchanger and a spiral fins type heat exchanger. The heat exchanger was inserted into a ceramic tube, made of alumina and a steel housing tube. This study by Avdic et. al [23] demonstrates the limited emission of a 8 kW porous media burner. The final result was the modulation of the burner thermal power up to 1:8. air ratio number was in the range of 1.30 to 1.55. This allowed for higher modulation of the burner power with low emissions.

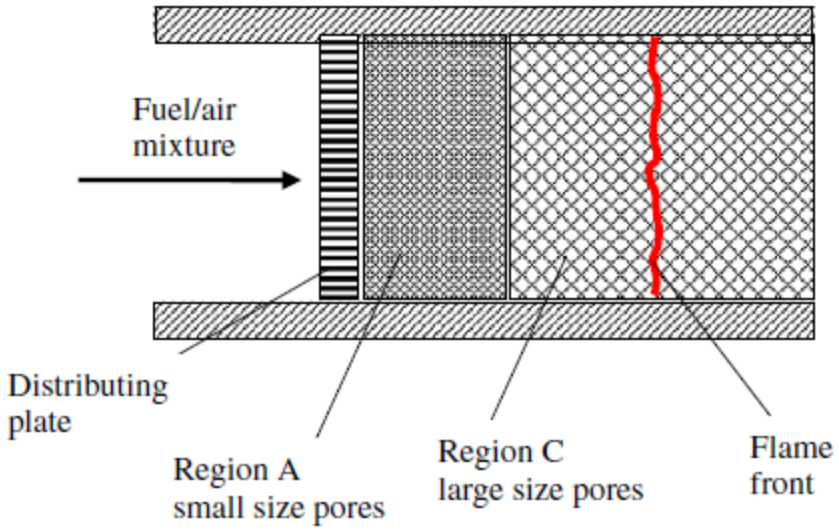

Figure 16) Schematic of a porous media burner used for household heating

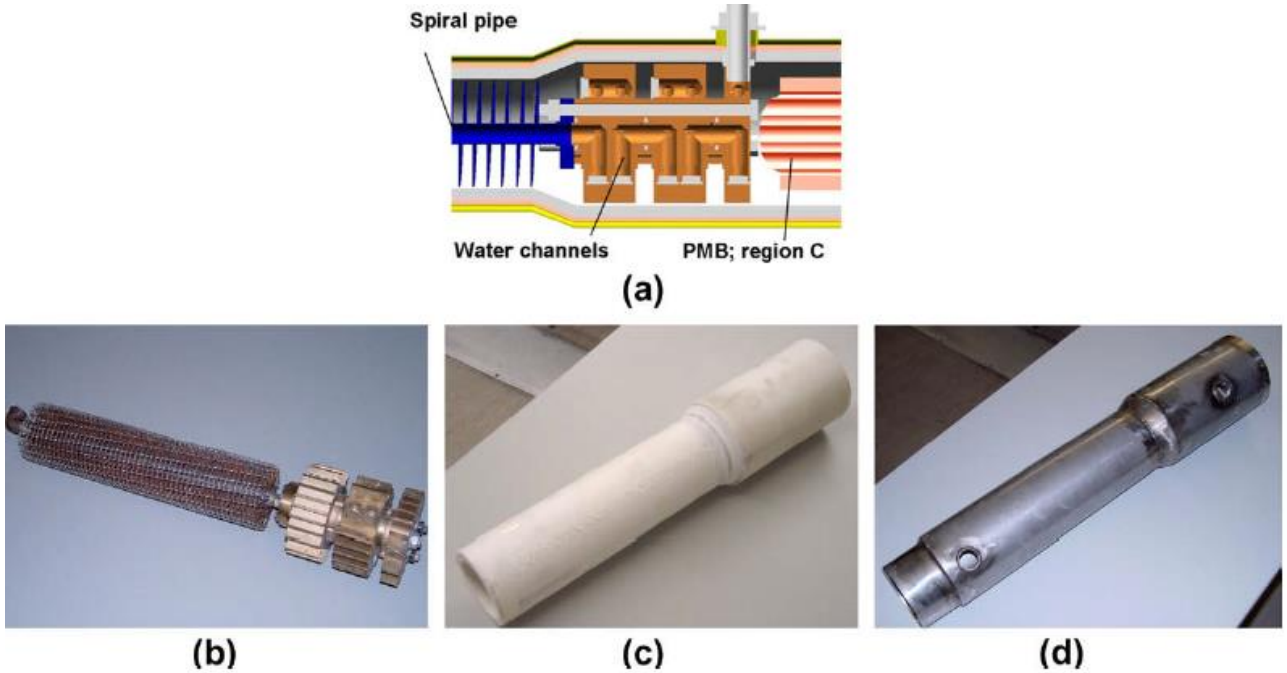

Figure 17) a) Detailed view inside the heat exchanger elements b) heat exchanger c) ceramic tube d) steel housing

N. Delalic. Et al[17] conducted experiments to evaluate porous media burners with heat exchangers built in boilers. **The experimental set up (shown in Figure 19)** was mounted in a way that the gas mixture flows from the top to the bottom. This design allows for removal of condensate water at the bottom. The water vapor condenses and supplies its latent heat to the heat exchanger. The additional empty area between the mantle of the combustor and heat exchanger at the exit was filled with pebbles of ceramic to increase the heat transport between the exhaust gases. Gas flow was monitored by thermal and mass flow controller. The controlling process and measuring of necessary parameters and process values was done through a Data Acquisition System hooked to a PC. NO_x and CO concentrations were measured by gas analyzers in the exhaust. **The variation of thermal efficiency with excess air ratio was recorded (Figure 18).** Considering that part of the latent heat of water condensed from exhaust gases is transferred to water in the heat exchanger, the thermal efficiency observed is very good. The difference between LHV and HHV is the latent heat of the water vapor. Thus, it is recorded that the thermal efficiency goes above 100 % for the LHV case. The pressure drop observed for the exhaust gases is low, for small combustor powers (2 kW and 5 kW). But the value goes up to 1200 to 1700 kPA for the 9 kW.

Successful applications of low temperature (condensate) boilers depend on the heat exchanger. Construction of heat exchangers for smooth or ribbed tubes is popularly known.

Further development can be expected in the application of porous medium in boilers. The advances of porous media combustion with built in heat exchanger are as follows:

- High power density of the system (7 MW/m^3)
- Superior thermal conductivity and thermal capacity of Porous Media
- Stable functioning of the burner heat exchanger
- High efficiency of heat exchanger
- Through increased energy efficiency the CO_2 and NO_X emissions were lower.

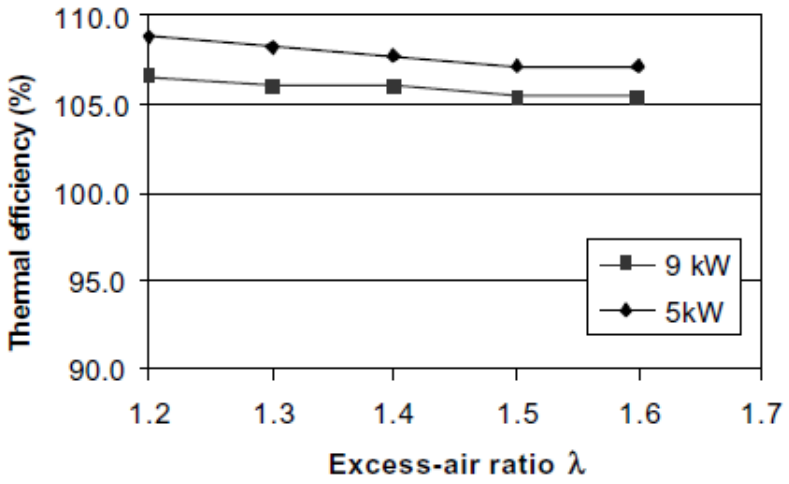

Figure 18) Porous burner -heat exchanger thermal efficiency relating to LHV

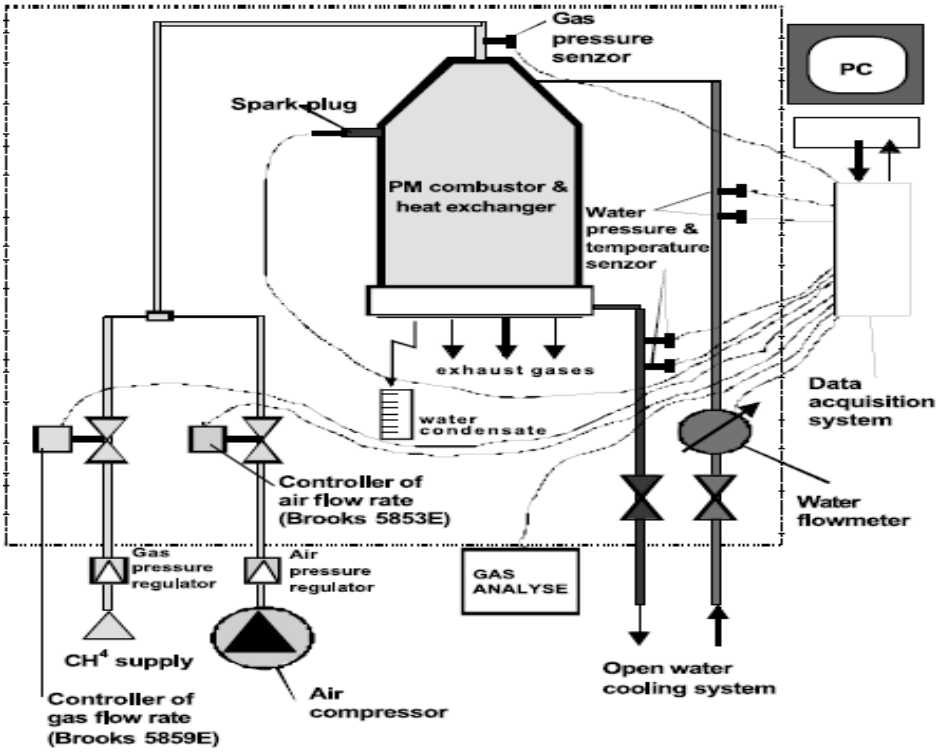

Figure 19) Schematic Diagram of Experimental Apparatus

2.8.CFD modeling of Heat Exchangers

A heat exchanger is a device that is designed to transfer heat from one fluid to another. The design of a heat exchanger is usually done using the following conventional methods:

a) LMTD- Log Mean Temperature Difference (LMTD)

b) έ-NTU (Number of Transfer Units Methods)

The above methods have been used for heat exchanger designs. These methods have certain shortcomings i.e. they are iterative and they require a prototype for implementing the design. Due to these reasons, these methods consume both time and money, especially for large scale models. However, economical access to greater computing facilities have led

to adoption of Computational Fluid Dynamics (CFD) for the design phase. CFD uses a simple principle of dividing the entire system in grids and analyzing by solving the governing equations on these discrete elements to obtain numerical solutions related to pressure distribution, temperature gradients, flow parameters. Due to lesser experimental work required CFD is cost-effective. Muhammad Mahmood Aslam Bhutta, Nasir Hayat, Muhammad Hassan Bashir, Ahmer Rais Khan, Kanwar Naveed Ahmad, Sarfaraz Khan have documented the key issues associated with the CFD design of heat exchangers in Applied Thermal Engineering Journal [9].

2.8.1. Flow Maldistribution

Non-uniformity in flow is a primary reason for heat exchanger performance. Faulty design of inlet/outlet port and header configuration, distributor construction are the causes for the non- uniformity. The following table compiled by Muhammad Mahmood Aslam Bhutta, Nasir Hayat, Muhammad Hassan Bashir, Ahmer Rais Khan, Kanwar Naveed Ahmad, Sarfaraz Khan[24], show how the maldistribution problem is employed by various turbulence models.

L. J. Shah et al (2003) studied the characteristics of vertical mantle heat exchanger which showed that the fluid distribution along the mantle is impacted by recirculation caused by buoyancy force in the mantle for high and low temperature inputs respectively. A Nusselt (Nu)-Rayleigh(Ra) correlation was developed, for which x is the distance from top of annulus:

$Nu_x = 0.46 \times (Ra_x \times \frac{x}{D_{hydraulic}})^{0.28}$, for $Ra = Ra_x \leq 10^{11}$ (2)

Momentum resistance modelling is a suitable method to analyze flow in finned exchangers. This conclusion was reached by A. Yashar et.al., modelled a four depth row exchanger to compare the air flow measured through CFD and the momentum resistance modelling method. [9]

2.8.2. Fouling

High temperatures or interaction with the exchanger walls may degrade the working fluid, which results in by products being generated that reduce the coefficient of heat transfer. Fouling may be reduced by cleaning periodically, which is not a very feasible option for automobiles Maria Valeria et al. 2009 studied the fouling rates with respect to velocities. The conclusion reached was that at higher Reynold's no.(Re) there is a drastic increase of fouling rate. To put things in perspective, a deposition of 1 g for Re= 1700 contrasts to a deposition of 22 g for Re =3700 as per this study.

2.8.3. Pressure Drop

Pressure drop, particularly due to the flow distribution devices in the heat exchanger like ports, headers, nozzles and ducts seriously affects the heat transfer rate.

Pedro F. Lisboa et. al. (2010) performed a CFD simulation using Fluent to analyze the impact of pressure on heat transfer rate for a heat exchanger used for producing supercritical Carbon di-oxide. Three different turbulence models k-ε, RNG k- ε and k- ε

were used. It was observed that for a rising fluid velocity with an aspect ratio set below the pressure drop was increasing. The results using RNG ,RNG k- ὲ showed a 10 % deviation from the Blasius solution and was closest to the experimental results.[24]

2.8.4. Thermal analysis

CFD has established itself as an effective tool for design optimization Yupeng Wu, carried out a model to study the effects of thermal performance of a heat exchanger, based on coil diameter and coil central interval difference. The following model was employed:

$$\frac{\partial(\rho T)}{\rho T} + \nabla.(\rho V.T - \frac{k}{c}\nabla T) = \frac{q}{c} \quad (3)$$

2.8.5. Shell Side Heat Transfer

In shell and tube heat exchangers the shell side flow is extremely complicated due to the presence of many leakage paths and bypass streams between different flow zones. However, the effects are not so prominent in small heat exchangers and hence all the leakage paths and bypass streams were neglected. Ender Ozden et. al carried out a numerical investigation for the shell side of a heat exchanger and compared it with analytical results. The desired mass flow rate and temperature values are assigned to the nozzle inlet of the heat exchanger. Zero gauge pressure is assigned to the outlet, to determine the relative pressure drop between the inlet and outlet. The baffle spacing is varied for different mass flow rates and the value of heat transferred as calculated from CFD data is compared with analytical solutions. It is obtained that the CFD data agrees

better with the Bell Delaware method than the Kern's Method of analytical solution.[25]. The Kern's method is a conservative approach and under predicts the heat transfer. The difference between the Bell-Delaware method and the CFD results increase with greater mass flow rate. The flow structures generated show that by increasing the number of baffles, cross flow windows are not well utilized and some recirculation regions formed. It is understood that the correlations' based approach is not bereft of weaknesses and the numerical analyses might help in pinpointing that area of weakness.

The pressure drop on the shell side of a heat exchanger is strongly affected by the baffle spacing. The ratio of the Baffle Spacing to the Diameter of the shell as used in quantitative analysis, predicts a lower pressure drop. Increasing the baffle spacing will reduce the pressure drop in the shell side of a heat exchanger.

2.9.Flow in Curved Conduits

Curved conduits can be used for heat exchanger design. Internal flow within conduits of constant cross section becomes more complex when a radius of curvature is introduced to the pipe centerline. In laminar conduit flow without curvature, the flow exhibits a velocity profile which is radially symmetric about the pipe centerline. However, for conduits with curvature, the maximum axial velocity shifts from the center toward the outer wall of the curved conduit. While such distorted velocity profile symmetry has been shown to increase, the total pressure drop through a given length of conduit, there is the benefit of increased heat exchange between the fluid within the conduit and the conduit wall. Such distorted velocity profile within the conduit may be attributed in viscous and inviscid

fluids to the centrifugal pressure gradient in the main flow acting on the fluid which is relatively stagnant near the conduit wall. In curved conduits, the ***Dean Number*** De, is used to characterize the relative influence of curvature on the velocity profile; where De is a function of ***Reynolds Number*** Re, ***curvature radius*** r_c, and the ***conduit flow radius*** R presented in Equation 4). **Velocity profiles for axial and secondary flows derived from the analytical solution for fully developed conduit flow with varying Dean numbers are presented in Figure 20.**

$$De = Re \cdot \sqrt{\frac{\mathrm{R}}{2 \cdot r_c}} \tag{4}$$

A numerical modelling of a double-pipe heat exchanger was conducted by T.J. Rennie et. al[26] for laminar flow and heat transfer characteristics under different fluid flow rates and tube sizes. Due to the secondary flow pattern in curved tubes, there is an additional convective temperature gradient in the flow. The objective of the work was to determine heat transfer characteristics, by varying input mass flow rates in the tube and the annulus of the double pipe heat exchanger and also vary the size of the inner tube. The boundary conditions associated with the inlets specified the inlet velocity along the axial direction. The outer surface of the heat exchanger was assumed to be adiabatic and the inner coil was set to allow conductive heat flow through its wall. The most important finding from the analysis is that the thermal resistance of the annular region of the tube is the most decisive factor for making a more effective design. Increasing the inner tube diameter reduces the

annular tube resistance. Overall heat transfer coefficients were calculated for Dean Number in the range of 38 to 360. The results show an upward trend in heat transfer with increased Dean Number. The annular Nusselt Number showed a linear relationship with the modified Dean Number. The modified Dean Number is the Dean number calculated for the annulus with a curvature ration of outer to inner radius. The Nusselt Number calculated was validated from literature. The results showed that both parallel and counter-flow had similar Overall Heat Transfer Coefficients. However, as expected there is an increase in heat transfer in the counter –flow direction.

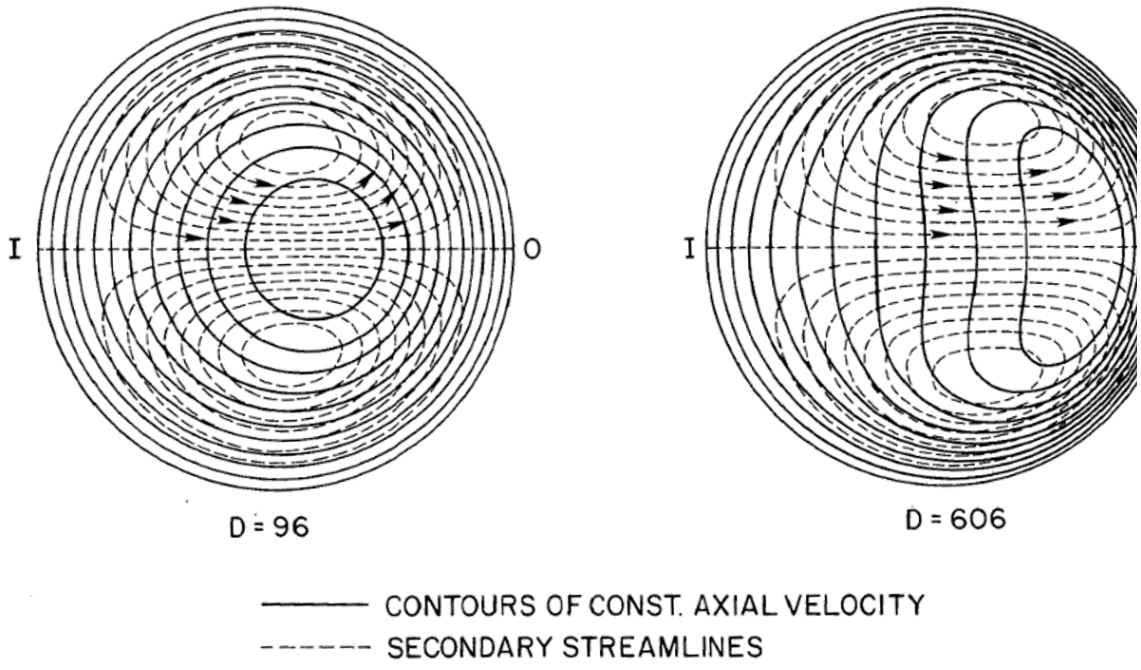

Figure 20) Axial velocity and secondary streamlines of flow within a curved conduit at various Dean Numbers. I and O denote the various Dean Numbers

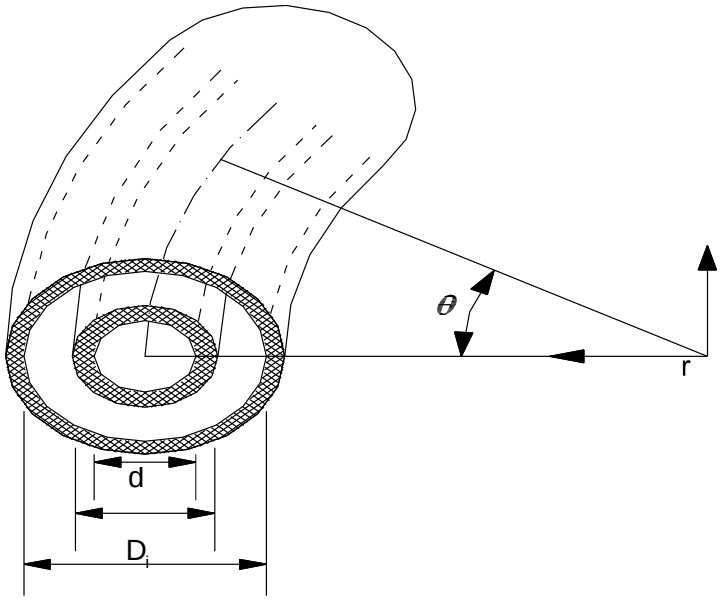

Figure 21) Double Pipe Heat Exchanger-Coordinate System

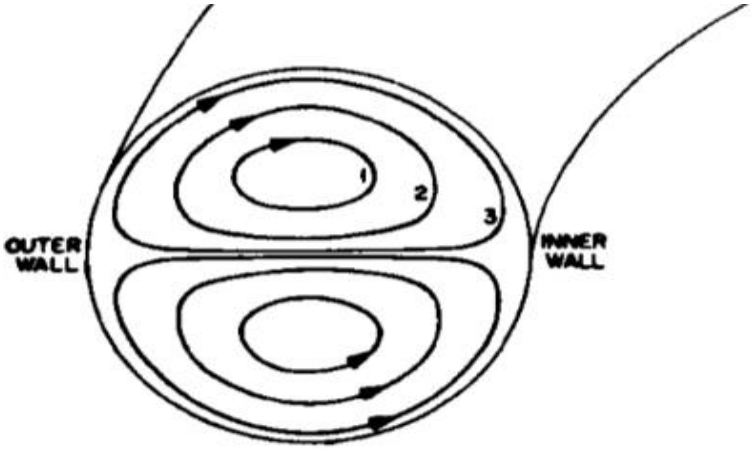

Figure 22) Secondary Flow in a Helical Pipe

The numerical analysis in[26] was verified by experimental results by T.J. Rennie et. al [27].The objective of the study was to design, build and instrument two double pipe heat exchangers. **Figure 21 shows the co-ordinates for a double pipe heat exchanger. Figure 22 shows the secondary flow phenomenon in a helical pipe.** The wall boundary conditions however differed from the numerical analysis in[26].The study focused on measuring the temperature by varying input flow rate to both the annular region and the inner pipe for two different heat exchangers both in case of parallel and counter-flow. The experimental set up consisted of cold water being used for the annulus region and hot water being pumped internally through the coiled tube. Flows in both pipes were maintained by flow meter and metering valves. Overall heat transfer coefficients were calculated and heat transfer coefficients in the inner tube and annulus were determined using Wilson Plots. The Nusselt Number is calculated for both the inner and annular flows. **The Annulus Nusselt Number and its variation with the Annulus Dean Number is shown in Figure 23**. The overall heat transfer coefficients are similar for both parallel and counter-flow arrangements. However, the heat transferred is much more for counter-flow, due to the larger average temperature difference. The Nusselt Number for the inner tube agrees well with the experimental data for the, but there is a disagreement for the annulus. This can be attributed to the fact that water enters the annulus through a right-angled elbow, which is very different to the flow conditions in the numerical model.

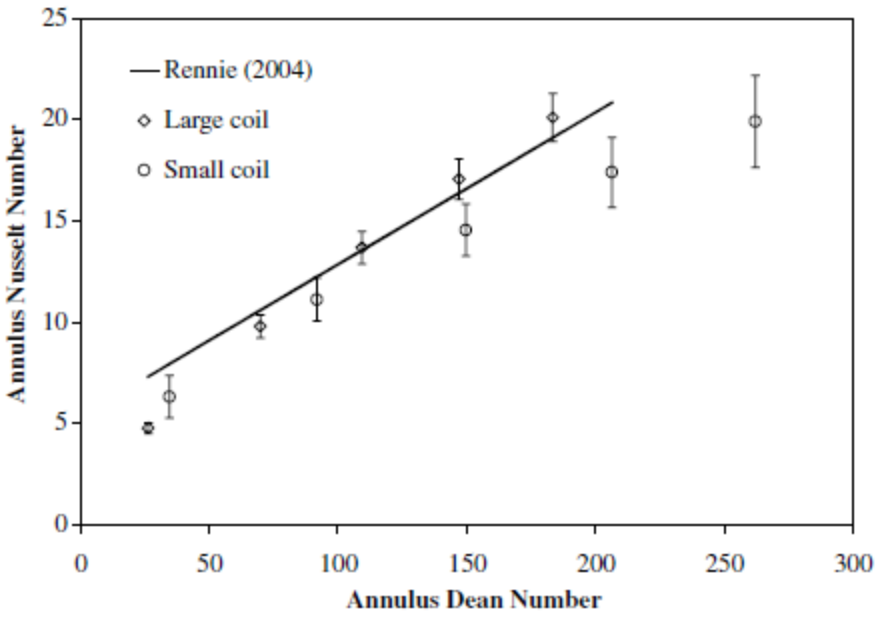

Figure 23) Annulus Nusselt Number and its variation with Dean Number

Van Der Vyer et. al [28] performed a CFD analysis for a tube-in-tube heat exchanger. The heat exchanger had hot water flowing in the inner tube and cold water in the annulus. The inner tube has a diameter of 8 mm, with an outer diameter of 10 mm. The inside diameter if the tube was 16 mm. Since steady state was assumed the heat exchanger was designed for a =n assumed length of 50 mm. The tube was made of copper with a conductivity of 386 W/K. Heat transfer values were determined from temperature values obtained from the analysis. The results were compared to the Dittus-Boelter correlation. The result shows an error of 4.6 % for the outer Nusselt Number and 18.8 % for the inner Nusselt Number.

The Dittus-Boelter correlation is as follows:

$$Nu = 0.023Re^{0.8}\ Pr^{n} \quad (5)$$

The study was also used to do CFD modelling and validation of a fractal heat exchanger. For inner flow good correlations were developed for friction factors over a wide range of Reynold's Number, 7500 to 18000. However, the annulus friction factors were not validated with the experimental results due to the limitations like bent flow at inlet and outlet of the annulus, differences in pressure measuring points between CFD and the experimental setup.

Pressure drop and heat transfer study in tube-in-tube helical heat exchanger [29] was investigated with experiments carried out in the counter –current mode, with hot fluid in the tube side and cold fluid in the annulus. Experiments were carried out by varying the flow rate both in the tube as well as in the annular region. **Figure 24 shows the variation of Overall Heat Transfer Coefficient with Outer Dean Number. Figure 25** shows the variation of Overall Heat Transfer Coefficient with Inner Dean Number. It was observed that the overall heat transfer coefficient increases with increase in the coiled tube Dean Number, when the flow rate in the annulus region is constant. Similar trends were observed for different flow rates in the annulus region for a constant flow rate in the coiled tube.

For a long helicoidal pipe heat transfer correlations were developed by experimental investigations.[30] The process was condensation of R 134 refrigerant in a helicoidal pipe by cooling water outside. The cooling water for mass fluxes were increased ranging from

100 to 400 kg/m^2, for a Reynold's Number range ranging from 1500 to 9000. The heat transfer coefficient for R134a for different coolant flow rates have been analyzed. It was found that the average heat flux of the refrigerant flow trends upward for an increased with the water flow rate; i.e., the heat transfer coefficients on the refrigerant side decreased as the mass flux of the refrigerant flow increased. **The experimental set up is shown in Figure 26.**

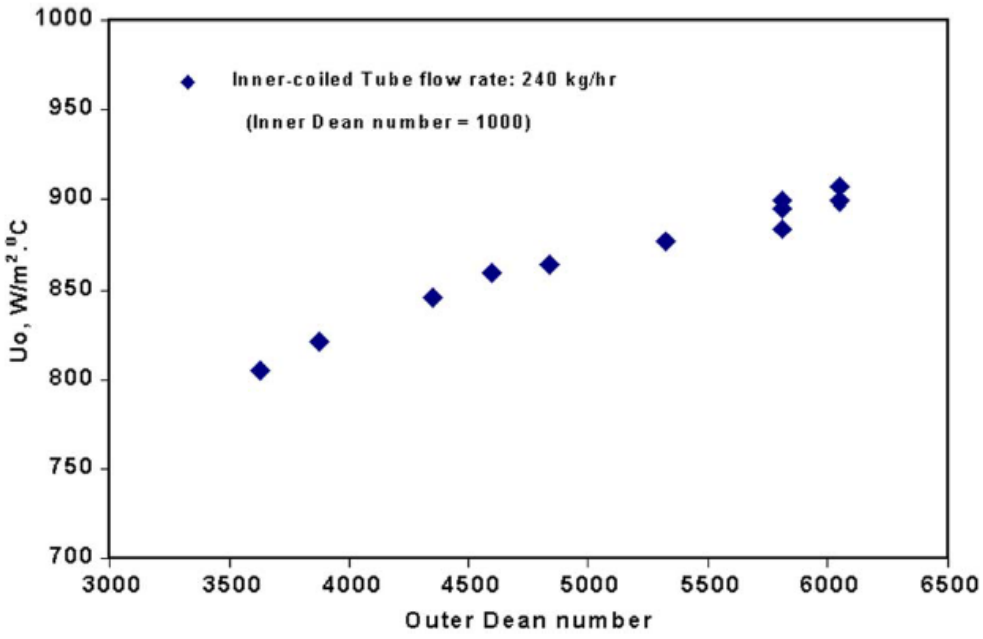

Figure 24) Variation of Overall Heat Transfer coefficient with Outer Dean Number

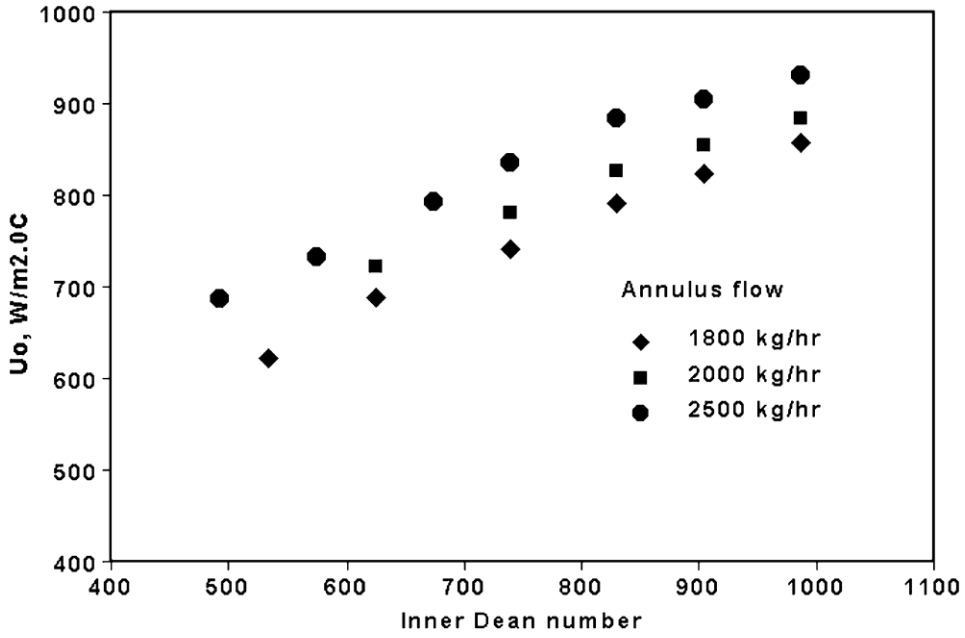

Figure 25) Variation of Overall Heat Transfer Coefficient with Inner Dean Number

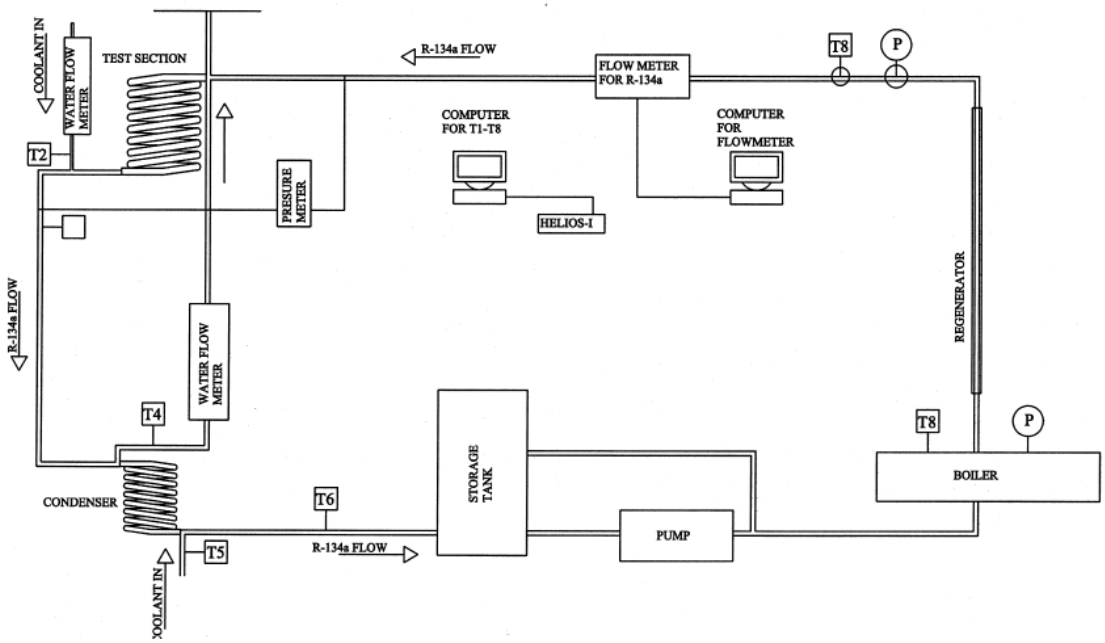

Figure 26) Experimental set up for heat transfer in R134a for a helicoidal pipe

2.10. Heat exchangers with helically coiled tube

Naphon et. al reported a literature review of study of pressure drop and heat transfer in curved tubes.[31] There are two specific types of configuration of curved tubes-Helically Coiled Tube and Spirally Coiled Tubes. For helical coil tubes, numerous theoretical and experimental works have been reported. For, spiral coil tubes, very few papers have been reported and only one of these papers presented the correlation of the in-tube heat transfer coefficient. In addition, none of the papers presented the flow characteristics and pressure drop. For other curved tubes, single-phase, two-phase heat transfer characteristics and single phase heat transfer characteristics have been numerously presented. The literature for experimental and CFD modeling of helically coiled tube heat exchangers is richer than spirally coiled Tube Heat Exchangers. In 2002 Prabhanjan et. al conducted an experimental study to compare heat transfer between straight and helical coil tube heat exchangers.[32].This was not the first study to compare the performance of these two types of heat exchangers. However, this was the first time that instead of boundary conditions like constant wall heat flux and constant temperature at the walls, the experiments were based on fluid to fluid heat exchange. The helical coil heat exchanger had 10 turns, 15.7 mm ID, no pitch and a tube wall thickness of 1.2 mm, helical diameter of 203 mm and was 6.3 mm in length, inserted in a mild steel pipe of 1287 mm diameter. The annulus of the straight tube is exposed to water at constant temperature. Similarly, the helical coiled tube is exposed to a bath of water at constant temperature. **Figure 27 and 28 compare the temperature and heat transfer coefficient respectively, for different flow rates at different bath temperatures.**

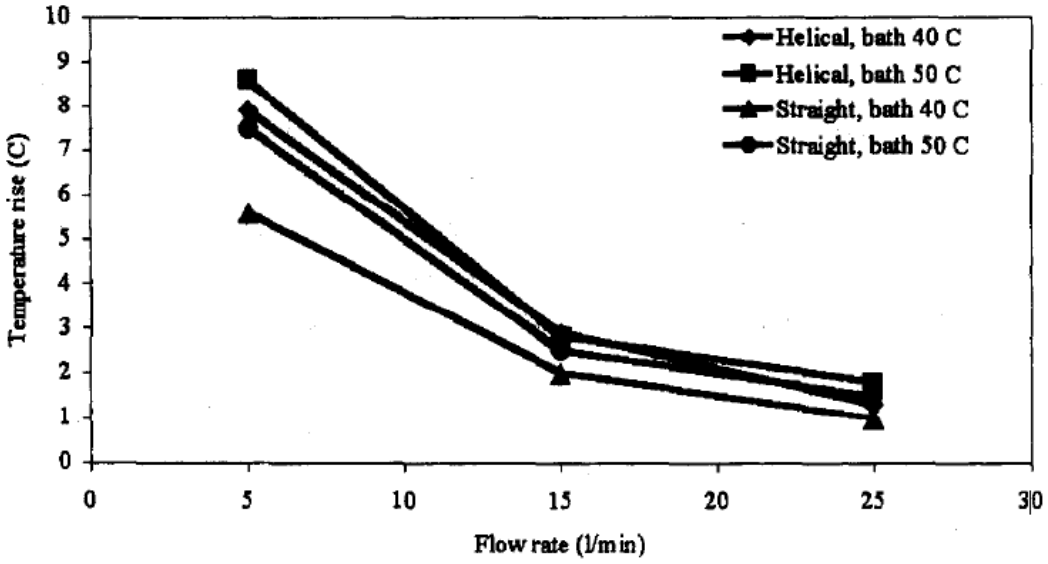

Figure 27) Temperature vs Flow rate for different temperatures of the helical bath for both helical and straight tubes for helical coil and straight pipe

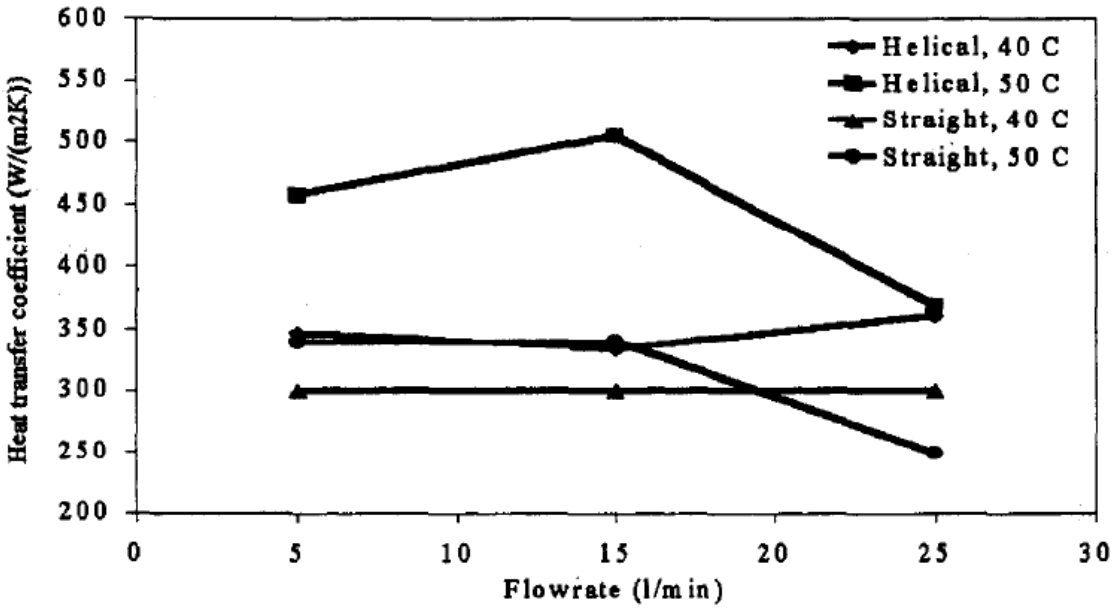

Figure 28) Heat Transfer Coefficient for different conditions of the hot bath for helical coil and straight pipe

The rise in temperature and heat transfer coefficient of the helical tube is higher than the straight tube under same conditions, for low flow rates, due to secondary flows in curved tubes. At higher flow rates this trend is reversed due to lesser residence time in the flow, leading to decreased temperature increment. In all cases the flow was in the transitional regime or turbulent regime with Reynold's Number ranging from 8300 to 41400 and 7700 to 38300, for flows in the helical coil and straight pipe respectively. Fluid from inside the tube is thrown through the tube center towards the other wall and then is returned to the inner wall region, in a curved pipe due to the centrifugal effects. In laminar flow this secondary flow enhances heat transfer and temperature uniformity, due to greater mixing. Developing fluid-to fluid helical heat exchangers require a greater understanding of the physics associated with the flow, than applying the standard heat transfer boundary conditions. There have been many investigations regarding the heat transfer coefficients inside a coiled tube, but not many for the outside flow. Prabhanjan et. al [33] correlated the outside Nusselt Number with the Rayleigh Number, for coiled tubes in water using different characteristic lengths. The experimental set up, consisted of four coils, through which the fluid was pumped. Coil 1, 2, 3 were used to develop the Nusselt –Rayleigh correlations and Coil 4 was used to validate them. The speed of the pump motor was varied to obtain flow rates, corresponding to a Reynold's number range of 12000 to 27000. The coils were housed in a water bath and heated K type thermocouples were used to obtain the temperature at outlet, from which the Nusselt number was calculated. The Nusselt Number and the Rayleigh number were correlated using a power law relation and the coefficients

obtained by changing the characteristic length. The correlations developed did not have the highest coefficients, but were useful in developing a prediction model that favorably predicted outlet temperatures of the heat exchanger, as compared to experimental data for a particular set of mass flow rate, coil size, length and the bath temperature values

Jayakumar et. al modelled a helical pipe using the Fluent Code and validated it with experimental results. Most of the investigations on heat transfer coefficients have been done for idealized boundary condition. This investigation however focusses on fluid to fluid heat transfer and establishes that conjugate heat transfer gives more accurate results than constant wall temperature or constant heat flux boundary conditions. In contrast to previous analyses the heat transfer between hot fluid and cold fluid is modelled considering both inside and outside heat transfer coefficients. Fluid properties like C_p, μ, k, ρ have conventionally been used as constant inputs for analysis. Jaykumar et. al [34] used regression analysis and experimental data to correlate the fluid properties as functions of temperature. Thus, the analysis was carried out with variable values of the fluid properties, thereby capturing the changes in temperature during the heat transfer process. The pipe used for the experimental set up was 12.7 mm in OD and had a tube material of SS 316. The pitch circle diameter of the coil is 300 mm and the tube pitch is 30 mm. The helical coil is enclosed in a vessel to simulate the shell. A CFD analysis was carried out both for the conventional boundary conditions and also a fluid to fluid heat transfer was considered. The temperature and velocity profiles, at the tube exit showed that both for constant and variable properties of the fluid, there was an increase in value of both temperature and

velocity in the outer section of the pipe, due to centrifugal effects. The inner and outer walls of the pipe were defined as coupled for energy transfer. The inner and outer wall of the shell were taken as no –slip condition. Pressure velocity coupling for the model was resolved using SIMPLEC algorithm. The application is meant for turbulent regimes 2000 to 12000 and Prandl Number 1.0 to 3.5. **Figure 29 shows the profiles of velocity and temperature at the end of the helical coil both for constant and variable temperature properties.**

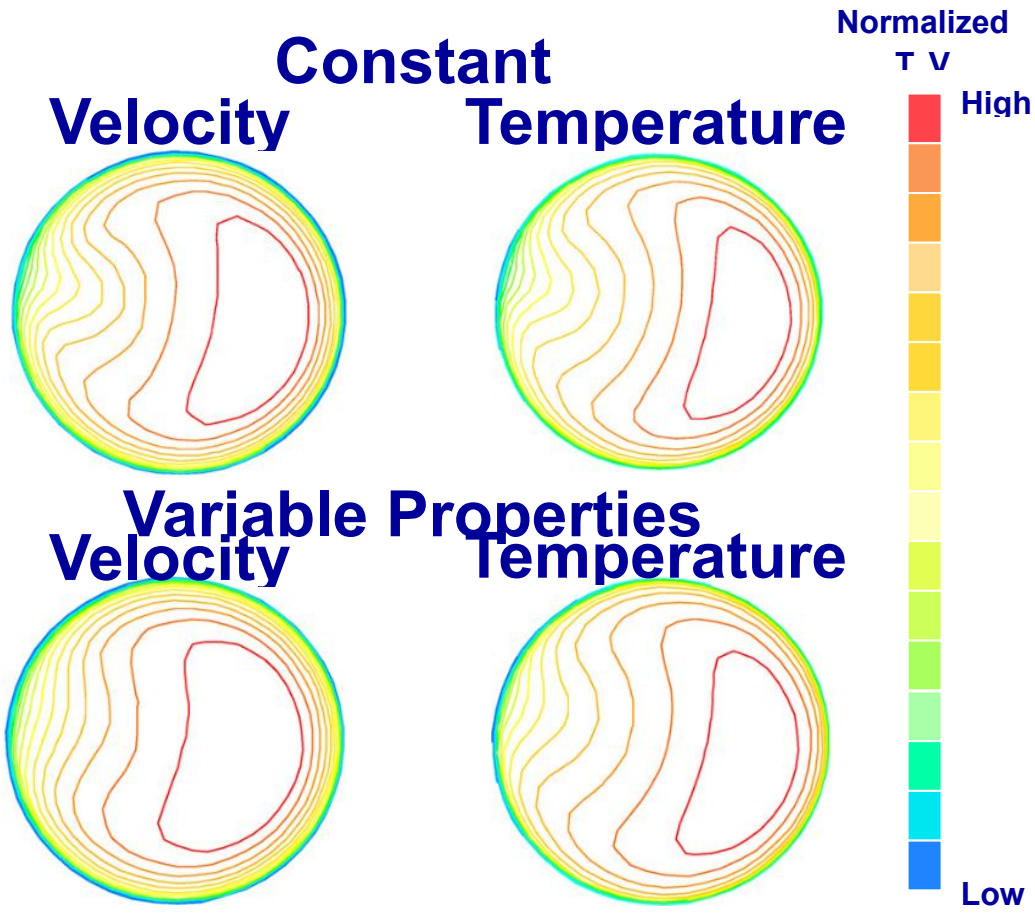

Figure 29) Velocity and Temperature Profile in a helical tube

2.11. Two phase flow in a helically coiled tube heat exchanger

A reactor was modelled using an experimental set up with helical coiled tubes [35] with the design parameters as follows:

a) The steam pressure was 5 MPa.

b) It has long superheated region to keep the steam at superheated condition under varied operating conditions.

The pressure vessel in the test rig was simulating a water reactor. It has a 0.8 MW heater simulating a reactor core, a steam generator with helically coiled heat transfer tubes and cover portion filled with Nitrogen Gas at the upperpart in the pressure vessel. Primary water from a circulating pump enters a pressure vessel, heats up the secondary water in the steam generator, is heated at the heater and is returned to the pump. Secondary water is cooled in a cooler. The coil is 595 mm in diameter and the tubes are of 14.3 mm ID. The real reactor coil has diameters of 2430 and 4522 mm. It is understood that the centrifugal effects due to curvature in the model, which is much smaller than the reactor will be more pronounced. It was observed that in the boiling region the heat transfer was not affected much by the curvature of the tubes and correlations for straight tubes could be used. Dry out at greater than 90 % shall be carried out for the evaluation of heat transfer properties. Pressure drop increases both with increase of mass flow rate and decrease of steam pressure. Pressure drop decreases with the increase of heat flux.

2.12. Simulation of Heat Transfer in Boilers

The most widely available example of phase change heat exchanger are the power boilers. A power boiler consists of convection and radiation zones. In a power boiler the convection zone [36] accounts for around 50 % of the cycle heat generated and hence there is an interest level in modelling fluid flow and heat transfer in this zone .An accurate model can provide significant assistance in improving the efficiency and durability in this zone. Antonio Gomez et. al [36] simulated the temperature of the fluid in the tube at different loads (in percentage of the boiler).**The calculated and measured exchange heats for**

various loads were compared and presented in Figure 30. Figure 31 shows the CFD simulation of temperature distribution in the convection zone of a power boiler.

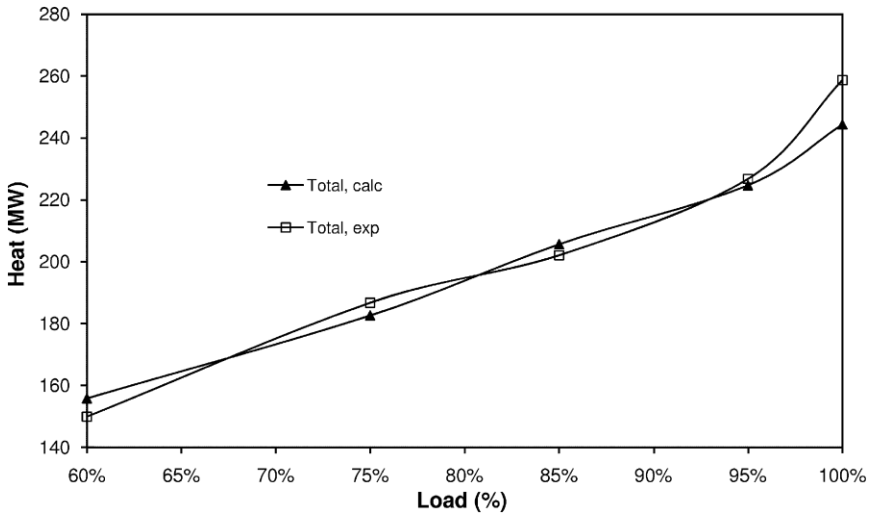

Figure 30) Heat at different loads

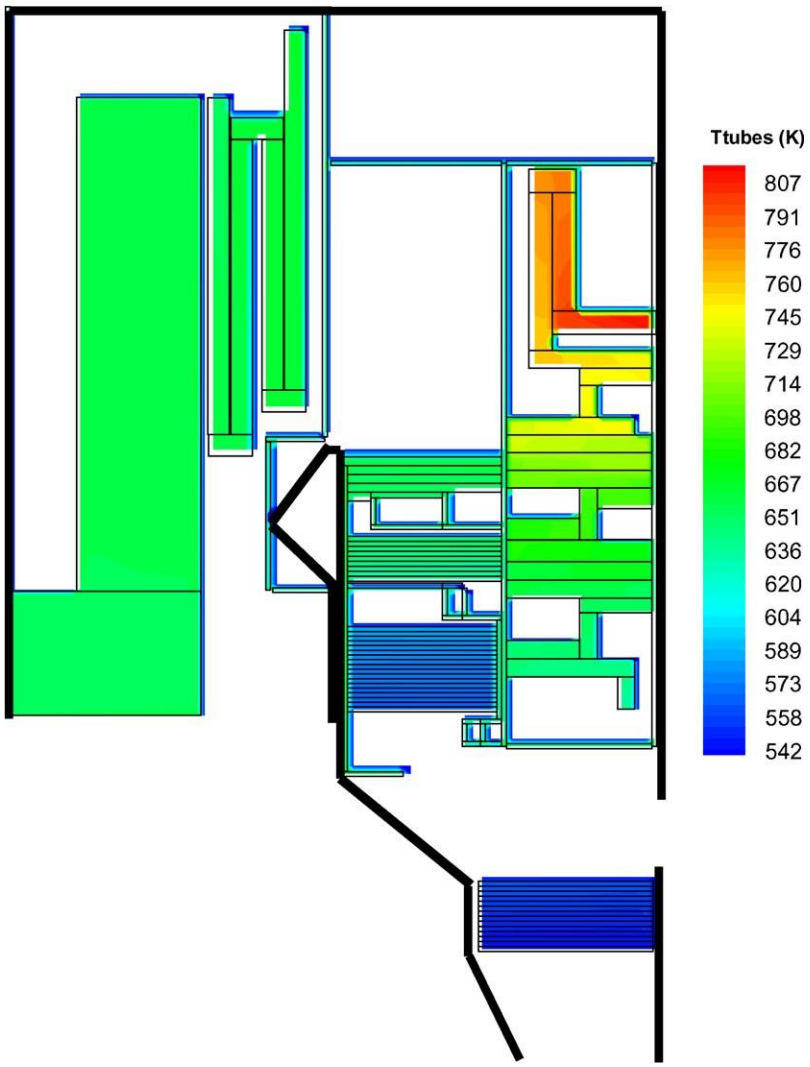

Figure 31) CFD simulation of temperature distribution in the convection zone of a power boiler

CHAPTER THREE: SYSTEM DESCRIPTION AND OVERVIEW

The process schematic for the entire automobile power plant is shown in Figure 32.

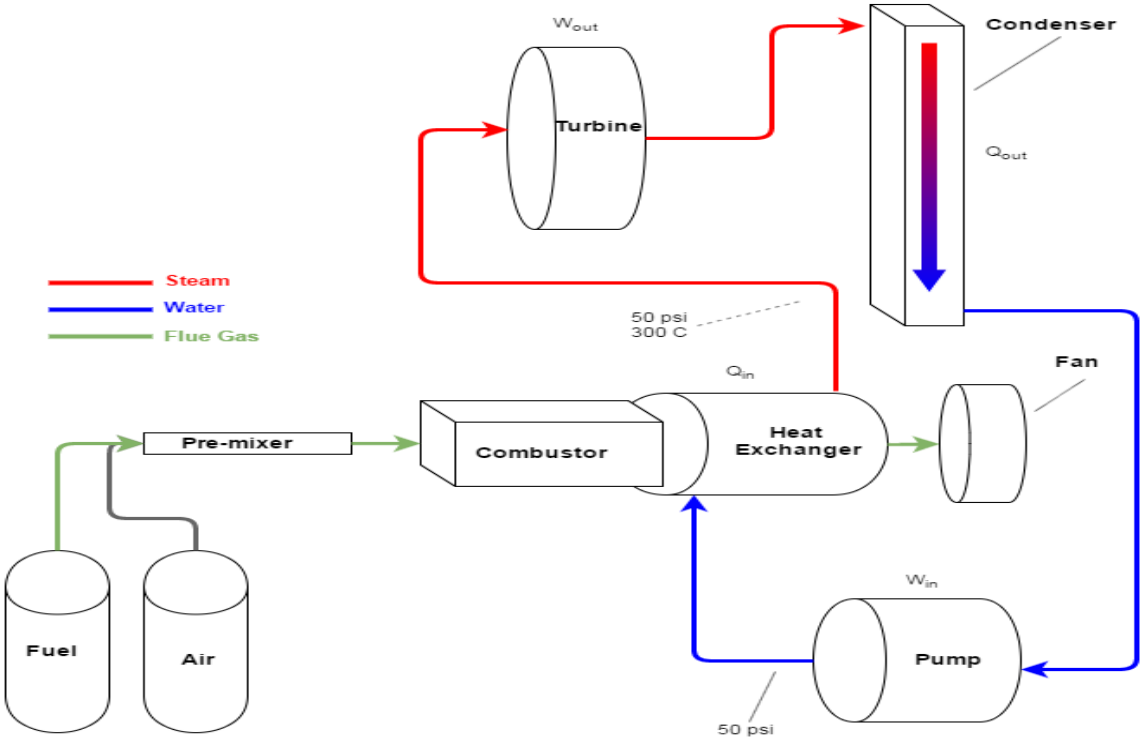

Figure 32) Process Schematic

The system consists of an Air and Flue Gas Path and a Steam and Water Path. The most convenient way of visualizing such a system is a Piping and Instrument Diagram (P&ID), which shows all lines and instruments.

3.1. Air and Flue Gas Path

Air is delivered to the combustor through a FD fan, with a control damper downstream to it to vary the airflow rate. The fuel is pumped from the fuel cylinder through a control

valve. We have provisions for both liquid and gaseous fuel. The fuel and air will be mixed in a pre-mixer and the mixture will be charged into a combustion chamber containing porous material. The heat exchanger is of annular design with the flue gases of combustion flowing from the combustion chamber into the heat exchanger and water tubes spiraled in the annulus. Thus, heat is transferred from the hot gases to the water to generate steam. The boiler is selected as a water tube heat exchanger. Fire tube boilers have large water volume and hence take more time to reach the required pressure and start up. The furnace will be designed for a hot gas temperature of 900 C. The furnace will be maintained at a draft of -2 to -5mm WC. The pressure within the furnace shall be maintained by adjusting the control dampers at inlet of the ID fan and outlet of the FD fan. The boiler furnace temperature and draft shall be controlled as per the load and its fluctuations. P&ID of Air, Fuel and Flue Gas along with legends is shown in Figure 33. The Piping & Instrument Diagram for Water and Steam Path, is shown in Figure 34.

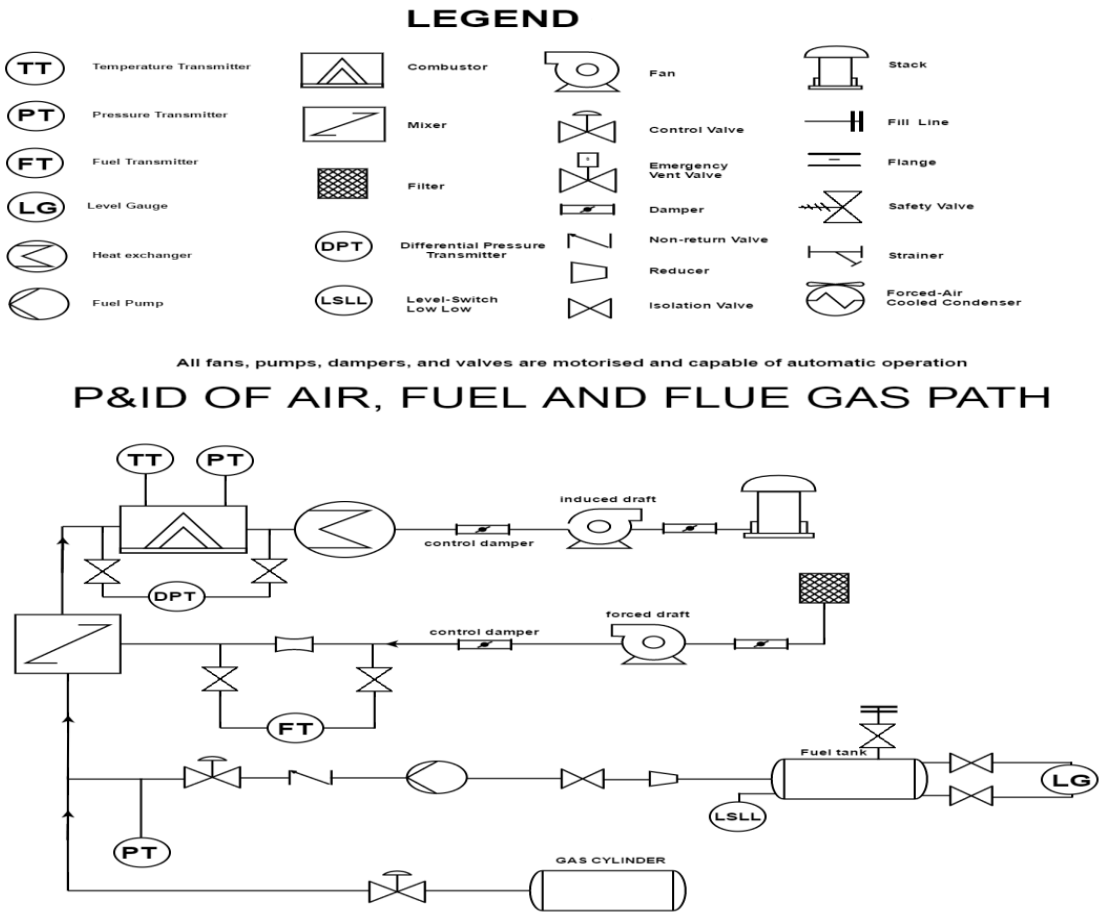

Figure 33)Piping and Instrumentation Diagram of Air, Fuel and Flue Gas Path

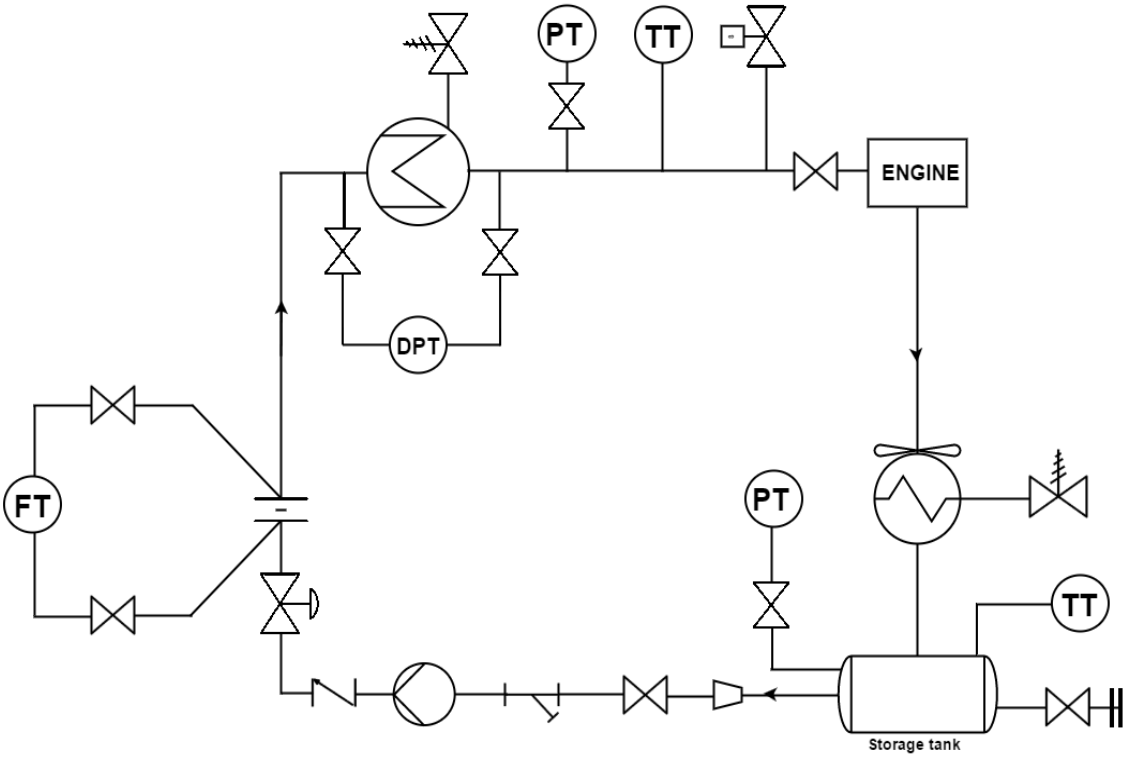

Figure 34) Piping and Instrument Diagram of Water and Steam Path

3.2. Water and Steam Path

The steam from the engine will be condensed in a Forced Air Cooled Condenser wherein the steam will be condensed at 14.7 psia, atmospheric pressure, 100º C. The condensed water will be stored in a Storage Tank and pumped by the Feed Pump to be fed in the heat exchanger. The heat exchanger coils and the condenser shall have safety valves for protection. There shall be connections to fill distilled water into the storage tank.

3.3. Control Philosophy

3.3.1. Furnace Draft Control

The Furnace draft is to be maintained between -2 to -5 mm wc, to ensure proper combustion and a slightly negative pressure in the furnace. The controller shall receive the signal from the Differential Pressure Transmitter across the furnace which will actuate the control damper in the ID Fan. In this way. the draft can be regulated.

3.3.2. Combustion Control

The signal of the pressure transmitter at the outlet of the steam line from the heat exchanger is fed to the controller. If the value falls below the set point the Flow Control valve (FCV) in the fuel line and the control damper of the FD fan are opened more to push up the steam pressure to the set value.

3.3.3. Control Logic

- All pumps shall take suction from reservoirs or tanks. To prevent dry run, level switches will be incorporated in the tanks, which will be interlocked with the pump motors to allow auto-stop to avoid dry run.
- All valves, dampers, motors shall be automatically operated by motor or pneumatic cylinders. Trip of ID fan will trip all other motors and valves/dampers.

- To save the system from catastrophic accidents the gate valve for isolating steam from the engine shall be automatically closed when the engine is shut down. The signal shall come from the Engine Governor to actuate the valve via the Boiler Controller.
- In case of emergencies the governor shall automatically actuate the vent valve in the boiler to prevent accidents.
- The controller shall be designed to follow the sequence of operation automatically as the car is started:
    a. ID fan motor started, water and fuel (in case of liquid fuel) feed pumps started
    b. ID Fan damper opened
    c. FD fan motor started
    d. FD fan damper opened
    e. Air and fuel control valves/dampers opened

3.4. Combustion Chamber

The combustion chamber is intended to be utilized in conjunction with a porous ceramic solid of ZrO_2 or Al_2O_3 with a porosity of 10 pores per inch solid length of 2.00" and outer diameter of 2.00" with or without catalytic coatings. Fuels for said combustor may be in either liquid, as Gasoline, Diesel, Bio-Fuel Blends; or gaseous as CNG, methane, or syngas. The design of this combustor shall outline the following points of logic:

- Ease of Ignition
- Reliable and Safe Operation

- Short Warm Up Times
- Specific Performance
- Stable Operating Ranges
- Ease of Manufacturing/Assembly/Maintenance
- Throttle Response

The combustion chamber presented herein is intended to convert fuel to heat at a minimum rate of 75 kW, when using methane fuel, with a flue gas temperature of 900 °C. This combustion chamber is intended to be used with a heat exchanger, to convert liquid s water to a superheated vapor. The ability of this combustor to operate on liquid fuels is achieved by an in-line tube mixer in conjunction with a solenoid actuated spray nozzle which is capable of actuation in the sub 10 kHz range for efficient fuel mixture control and low emissions.

3.5. Material Selection Philosophy

3.5.1.Steam Pipes: SA 106 Gr. B

This is a type of Carbon Steel. **The composition is given in Table 3** and is selected as per the process temperature of 300º C.

Table 3) Composition of SA 106 Gr B

Constituent	**Composition**
Carbon max. %	0.30

Constituent	**Composition**
*Manganese %	0.29 to 1.06
Phosphorous, max. %	0.035
Sulfur, max. %	0.035
Silicon, min.%	0.10
Chrome, max. %	0.40
Copper, max. %	0.40
Molybdenum, max. %	0.15
Nickel, max. %	0.40
Vanadium, max.%	0.08

3.5.2.External Gas Pipe: Mild Steel ERW

Since the gas pipe will not be exposed to very high pressures (the furnace will be maintained at a pressure of -5 mm wc and the pressure will remain negative during normal operating conditions. So, MS ERW pipes are suitable for the gas path and the combustor shell.

3.5.3.Boiler Heat Exchanger tubes (steam path): SS 304

3.5.4.Condenser tubes: SS 304

3.5.5.Raw water inlet pipe: SS 304

3.5.6.Condensate Storage Tank: PVC or SS304

The make -up added to the cycle in the Storage Tank will be Distilled or De-mineralized water. This is essential to prevent oxidation and damage of steam pipes and tubes at high temperature. This water when used at atmospheric temperature shall be fed through pipes and stored in tanks, made of material which does not react. De-ionized water is hungrier for ions than untreated water and hence it is very important that this kind of treated water be used only with materials which do not react like PVC and other plastic based materials or Stainless Steel. **SS304 (composition is shown in Table 4)** is selected for this duty for tanks and pipes

Table 4) Composition of SS 304

Constituents	**Percentage**
Ni	9.25
Cr	19.00
Si	1.00 (max)
Mn	2.00 (max)
C	0.080 (max)
P	0.045 (max)
S	0.030 (max)
Fe	Balance

CHAPTER FOUR: MODELING

4.1. Problem Description

The project is aimed at designing an optimal heat exchanger coupled to a combustor with porous media to evaluate a possibility of steam generation. Hot gases are generated by combustion of natural gas in the combustion chamber. The hot gases generated are used to heat water and generated steam. To fulfill the load, the heat exchanger design consists of a helical tube, which is divided into three sections was performed. The first section of the heat exchanger, the pre-heater *converts* water to a saturated liquid at 50 PSI, 300-degree C. The second portion consists of a phase change section where water is converted to saturated steam. The third section is the superheater where the saturated steam is converted to superheated steam. The design of the heat exchanger can be carried out by analytical methods. However, since the heat exchanger uses helically coiled tubes, it is not a standard empirical design and hence a numerical model is set up, for accurate prediction of results, where by the mass and momentum conservation equations are solved by Siemens NX Thermal-Fluid Code. The aim is to design the heat exchanger optimally so that the coil length is minimum and the surface area required for the heat transfer is minimized. It is assumed that the boundary condition for the phase change section is constant temperature of water, whereas the boundary condition for the pre-heater and superheater sections are constant heat flux from the flue gases, generated in the combustion chamber. The software

Siemens NX was used in this research work and the description of the software and its usage to build the model is provided in paragraph 3.2.

4.2. Description of Software

The software used for the analysis of the heat exchanger system is Siemens NX 9. The software has capabilities of creating of sketches, parts and manufacturing drawings. NX is equipped with an advanced simulation model with solvers for Thermal, Thermal Flow, Multiphysics and Structural problems. For the given problem, we are using the NX Advance Simulation Thermal–Flow solver. NX Advanced Thermal Flow offers the following capabilities:

a. Extend thermal solution capabilities from NX Thermal and NX Electronic Systems Cooling

b. Solve complex heat transfer phenomena with a comprehensive set of modeling tools

c. Reduce costly physical prototypes and product design risk through high fidelity thermal simulation

d. Greater insight can be obtained through coupled thermo-fluid multi-physics analysis using NX Advanced Thermal with NX Flow or NX Advanced Flow

e. NX integrated environment., consisting of sketches to simulation offer the flexibility to make quick design changes and provide rapid feedback on thermal performance

f. Use turbulence models like k-ε, mixing length etc. for analysis.

g. Use parallel and serial solvers for solving complicated problems requiring substantial numbers of elements.

The preprocessor consists of meshing (both 2D and 3D), assigning of materials and other properties. The post processor consists of the simulation menu, with flow boundary foundations, temperature boundary conditions, flow blockage and initial conditions as well as constraints. The used governing equations for building the model are described in paragraph 3.3

4.3. Equations

CFD analysis of the heat exchanger involves solving, the governing conservation equations for flow and energy. In steady state, the time dependent terms are dropped and so the simplified terms are shown below:

Conservation of Mass: $\nabla.\left(\rho\vec{V}\right) = 0$ (6)

where,

$\nabla=\frac{\partial}{\partial x}+\frac{\partial}{\partial y}+\frac{\partial}{\partial z}$

$\vec{V}$ = Velocity Vector

ρ = density

x- Momentum: $\nabla\,.\left(\rho u\vec{V}\right) = -\frac{\partial p}{dx}+\frac{\partial \tau_{xx}}{\partial x}+\frac{\partial \tau_{yx}}{\partial y}+\frac{\partial \tau_{zx}}{\partial z}$ (7)

where,

p= pressure

u = Velocity component in X direction

τ= stress

y- Momentum $. \nabla\left(\rho v \vec{V}\right) = -\frac{\partial p}{dy} + \frac{\partial \tau_{xy}}{\partial x} + \frac{\partial yy}{\partial y} + \frac{\partial \tau_{zy}}{\partial y} + \rho g$ (8)

v =Velocity component in Y direction

g= acceleration due to gravity

z- Momentum: $\nabla . \left(\rho w \vec{V}\right) = -\frac{\partial p}{dz} + \frac{\partial \tau_{xz}}{\partial x} + \frac{\partial \tau_{yz}}{\partial y} + \frac{\partial \tau_{zz}}{\partial z}$ (9)

w=Velocity component in Z direction

$$\nabla . \left(\rho e \vec{V}\right) = -\rho \nabla . \vec{V} + \nabla . (k \nabla T) + q + \emptyset \quad (10)$$

is the energy equation.

Where, T= Temperature

q= heat transferred

The dissipation function is given by,

$$\emptyset = \mu[2[(\frac{\partial u}{\partial x})^2 + (\frac{\partial u}{\partial y} + \frac{\partial v}{\partial x})^2 + (\frac{\partial u}{\partial z} + \frac{\partial w}{\partial x})^2 + (\frac{\partial v}{\partial z} + \frac{\partial w}{\partial y})^2 + \lambda(\nabla.\vec{V}^2) \qquad (11)$$

where,

$\nabla = \frac{\partial}{\partial x} + \frac{\partial}{\partial y} + \frac{\partial}{\partial z}$

$\vec{V}$ = Velocity Vector

ρ = density

u = Velocity component in X direction

v =Velocity component in Y direction

w = Velocity Component in Z direction

T= Temperature

q = heat transfer

$\emptyset$ = dissipation function

The system is designed for an engine power input of 75 kW, based on small cars available in the market.

The steam condition at boiler outlet is 50 PSI, 300-degree C.

This corresponds to an enthalpy, h_3=3062 kJ/kg (from steam table).

Power at boiler outlet, $P = \dot{m}h_3$ (12)

Mass flow rate, $\dot{m} = \frac{P}{h_3} = \frac{75}{3062} \sim 88 \frac{kg}{hr}$ is the boiler steam requirement. With a 25 % margin the boiler capacity is designed at 110 kg/hr.

The engine shall be designed to expand the steam to atmospheric pressure.

So, the condenser outlet saturation temperature is 100 ºC, as per steam table.

For 100ºC boiler feed water the inlet enthalpy, is h_2= 418.991 kJ/kg

Thus, the total heat load on the boiler = $\dot{m}$ (h_3- h_2) = $\frac{110X(3068-418.991)}{3600} = 80.9$ kW

For 110 kg/hr, is divided into five input tubes, 22 kg/hr and a velocity (V) of 6.69 ft/s (assumed) for the economizer. The tube inner diameter (ID) can be calculated as follows:

$$\frac{\dot{m}\, v}{V} = \frac{\pi}{4} x {D_i}^2, \qquad (13)$$

where v= specific volume, V =velocity, D_i=Inner diameter

Tube ID in economizer is calculated as 1.72 inch.

The following boundary conditions are used for analysis in Siemens NX.

- For each feed water tube the mass flow rate is 22 kg/hr at input and output.
- For each feed water tube the input temperature is 100 ºC.
- For the economizer exit the constraint is 153 ºC which is the saturation temperature at 75 PSI, as per steam table.
- For the superheater, the steam temperature constraints are 153ºC and 300ºC at superheater outlet.

Table 5 below shows some of the design parameters.

Table 5) Design Parameters

Variable	**Parameter**	**Value**
P	Power of Engine	75 kW
$\dot{m}$	Capacity of Boiler	110 kg/hr
P_3	Steam Pressure at outlet of Heat Exchanger	50 PSI
T_3	Steam Temperature at outlet of Heat Exchanger/Superheater	300 Degree C
P_4	Condenser Pressure	Atmospheric
T_4	Condenser Temperature	100 Degree C
T_5	Temperature of water at outlet of economiser	153 Degree C
T_{g1}	Design Hot Gas Inlet Temperature in Heat Exchanger	900 degree C
h_3	Enthalpy of Generated Steam	3062 kJ/kg
h_2	Enthalpy of feed water	418.99 kJ/kg

4.4. Meshing

Several meshes were created as per the model to facilitate the analysis in Siemens NX. The flange of the **heat exchanger is made from the 2D mesh Shell1(visualization included**

in Figure 37) and the steam tubes are made from the 2D mesh Shell 3 (visualization included in Figure 36)). **Table 6 documents the properties of 2D Meshes.**

Table 6) Properties of 2D Meshes

Name	**Shell 1& Shell 3**
Type	Thin Shell
Material	AISI SS304
Type	QUAD8 Thin Shell
Size	0.1 inch

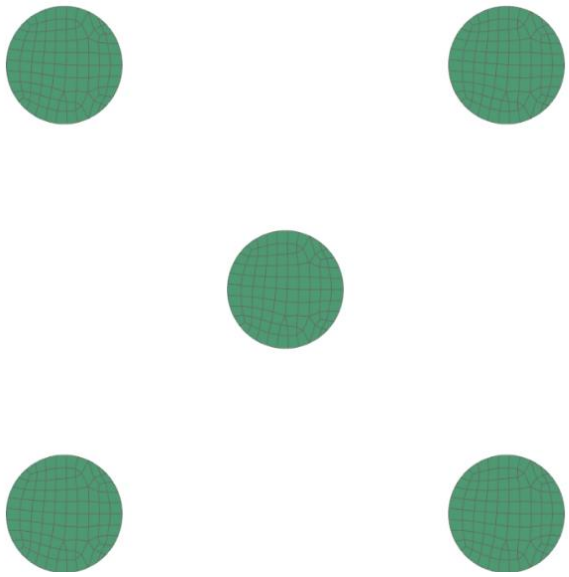

Figure 35) Visualization of Mesh Shell 3

The 2D meshes are extruded to form 3D meshes for the shell of the heat exchanger and the tubes. Solid (1) is the 3D fluid mesh representing the hot air path. Solid (2) is the 3D mesh for representing the water tubes and Solid (3) is the 3D fluid mesh representing the

water/steam in the tube. **Figure 38, 39, 40 are visual representations of 3D meshes Solid 1, Solid 2 and Solid 3 respectively**.

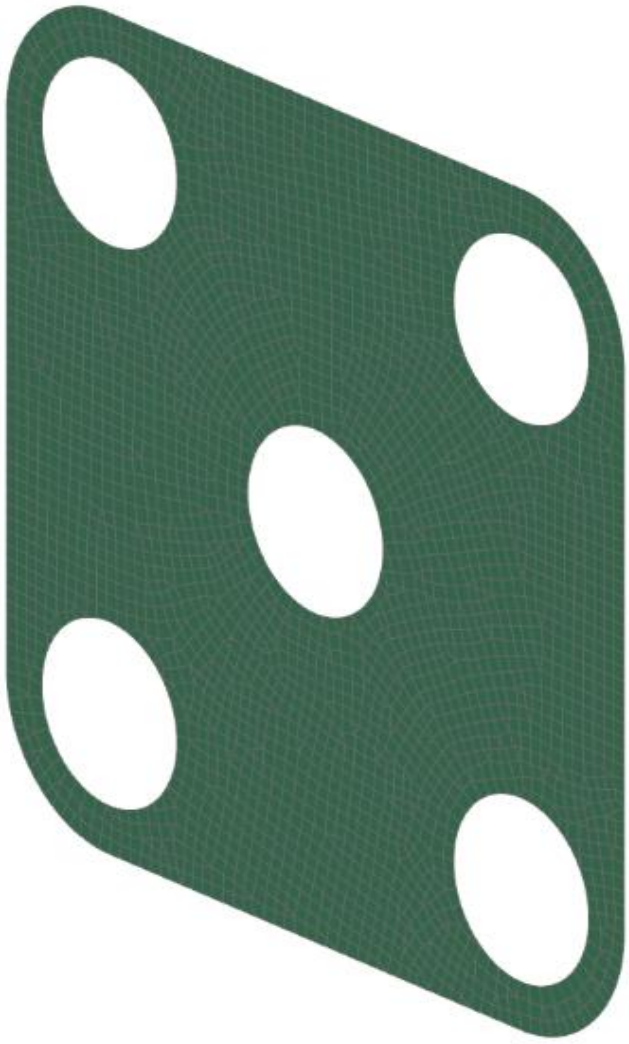

Figure 36) Visualization of Mesh Shell 1

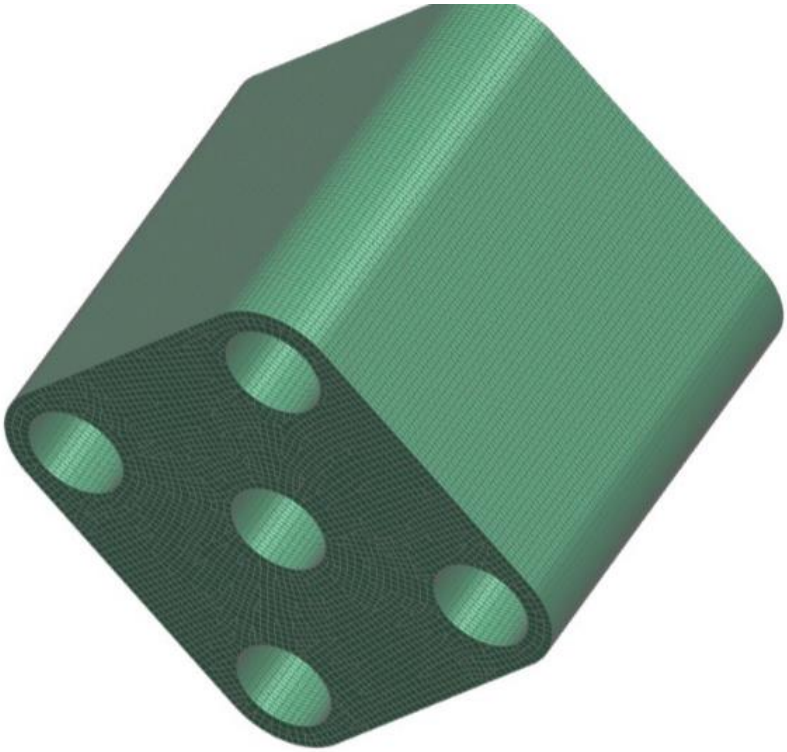

Figure 37) Visualization of 3 D Fluid Mesh Solid 1

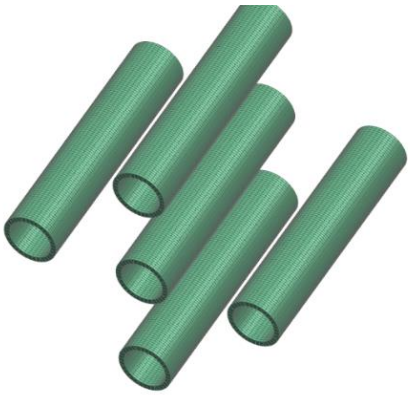

Figure 38) Visualization of 3D mesh Solid 2

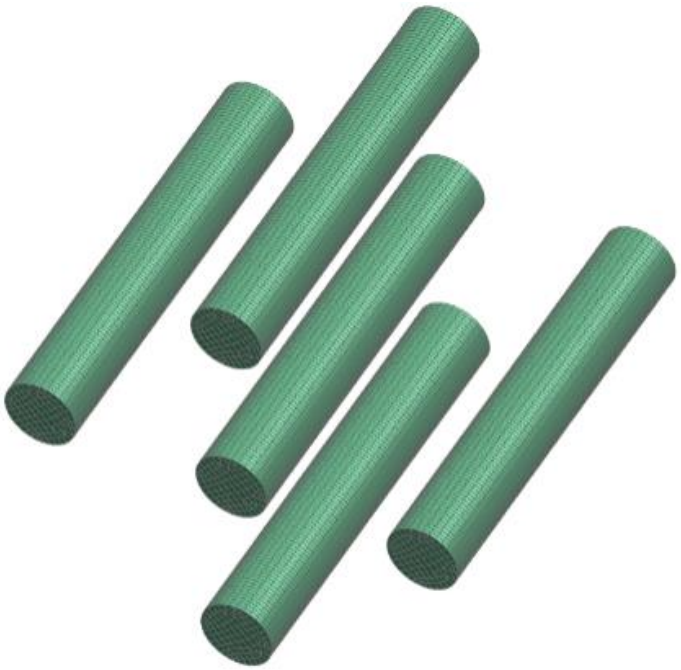

Figure 39) Visualization of 3D Fluid Mesh Solid 3

Table 7)Properties of 3 D extruded meshes

Name of Mesh	**Properties**
Solid 1	Material–Air Temperature Dependent Gas
Solid 2	Material-AISI SS 304
Solid 3	Material -Water/Steam

4.5. Model Geometry

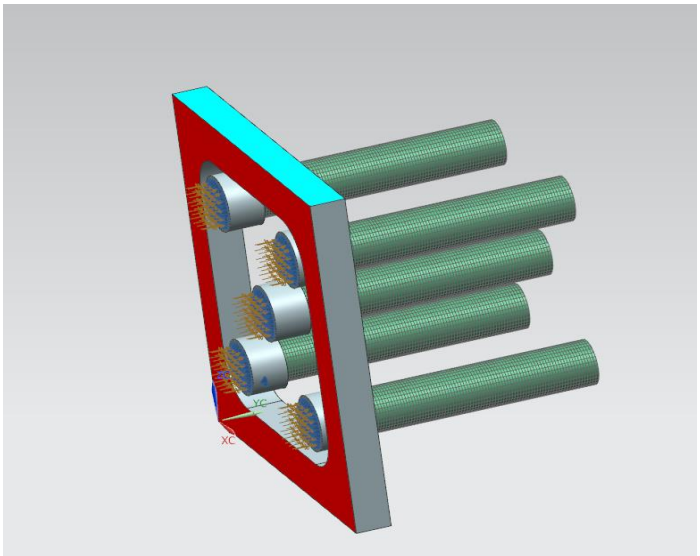

Figure 40) Visualization of straight tube heat exchanger model: tube side

Two designs were implemented and geometrical models generated for simulation in Siemens NX. One is the straight shell and tube heat exchanger. The heat exchanger is modeled as straight tubes of 1.72-inch Inner Diameter (ID) and material AISI SS304 (stainless steel) conveying water, housed within a shell. The shell consists of the hot gas path modeled as air temperature dependent gas as 8 inch x 8 inch. **The shell is depicted in figure 42 and is made of Mild Steel**. **The tube side model for the heat exchanger with straight tubes is shown in the figure 41. Figure 43 shows the two-dimensional side view flange of the heat exchanger with the tube sheet and holes for tubes.**

Another design used is the helical coiled tube heat exchanger. The heat exchanger is modeled as tubes in the form of a helix. A helical coil increases the heat transfer because

of the curvature effect and secondary flows resulting from it. The idea is to make a more compact heat exchanger using helical coils.

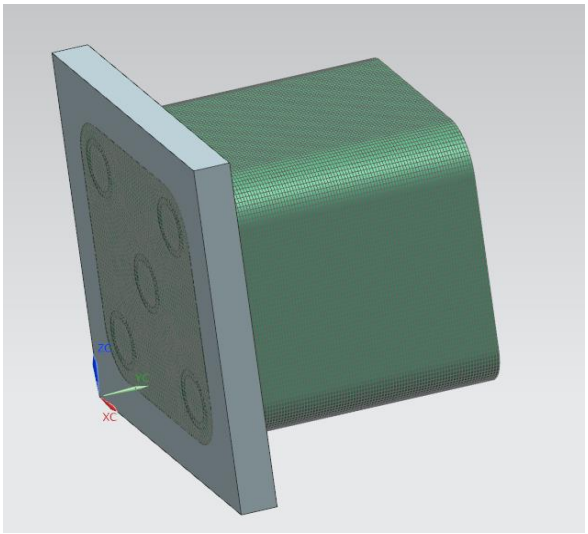

Figure 41) Visualization of Heat Exchanger Model: Shell Side

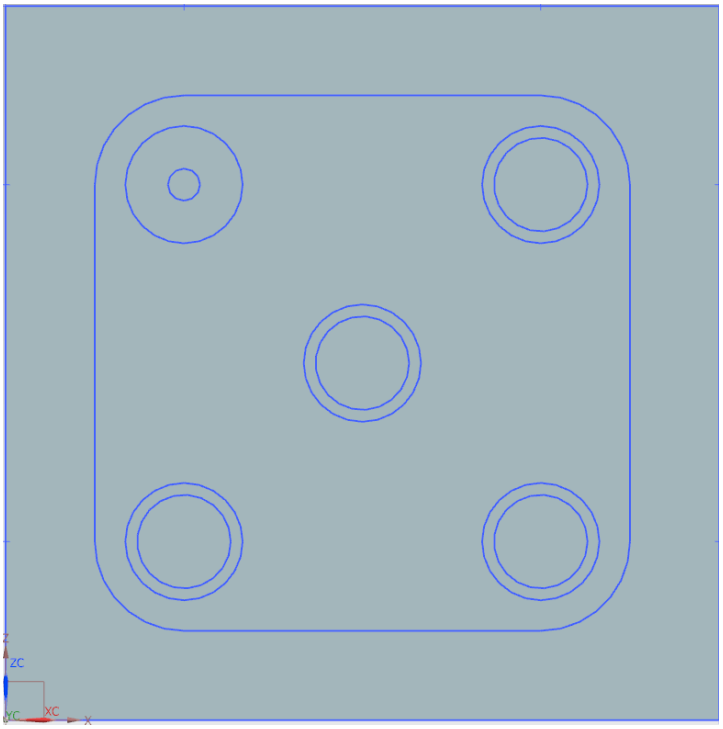

Figure 42) Side View of Heat Exchanger Model

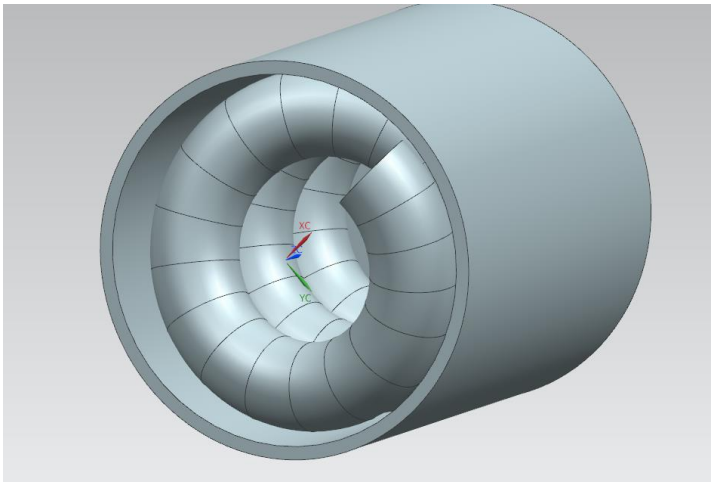

Figure 43) Model of Helical Coiled Tube Heat Exchanger

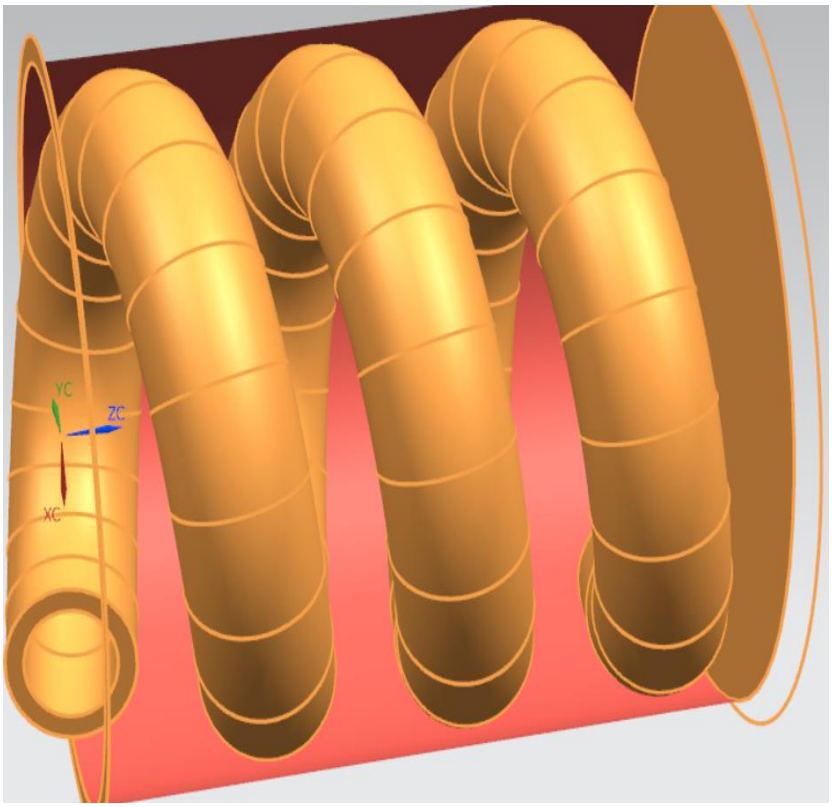

Figure 44) Section of Helical Coil Heat Exchanger

Figure 44 and Figure 45 depicts the model of a helical coil heat exchanger. This design consists of a water/ steam tube are housed within a shell of diameter. The hot gas from the combustor flows into the heat exchanger shell and heat is transferred to the helical coiled tubes. The tube has an inner diameter of 0.5 inch of schedule 40. The shell is made of Mild Steel and the tube is made of AISI SS 304.

CHAPTER FIVE: RESULTS

To facilitate design and easy analysis of the heat exchanger, a coupled thermal flow analysis is conducted only for a water single tube of the heat exchanger**. The geometric model is shown in Figure 46.**

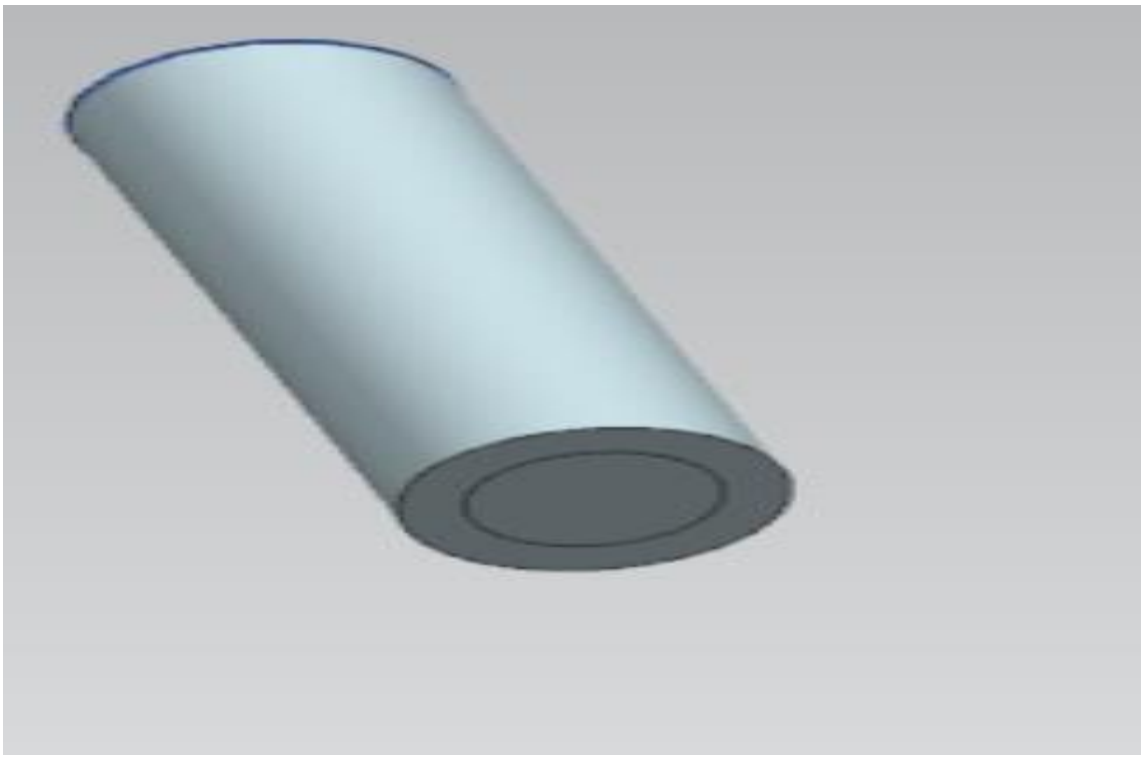

Figure 45) Geometric model of single tube of heat exchanger

Solver Type: NX Thermal/Flow

1. Analysis Type: Coupled Thermal/Flow
2. Number of nodes in thermal model: 194

3. Number of elements in fluid model: 508
4. Number of nodes in flow model: 126
5. Number of elements in flow model: 305
6. Number of fluid nodes reused for surface coating: 100
7. Number of elements created for surface coating: 412
8. Steady State Analysis Solution Method: Concurrent
9. Ambient Temperature 20 ºC
10. Ambient Pressure: 1.014 X10^5 Pa
11. Flow laminar/turbulent model: K-epsilon
12. Flow solver iteration limit: 1000
13. Advection scheme momentum: First Order
14. Advection scheme energy: First Order
15. Advection scheme K-epsilon: First Order

Table 8 lists the boundary conditions for thermal analysis.

Table 8) Boundary Conditions for Simulation

Boundary Condition	Type	Value
Thermal Load	Heat Load	16 kW
Temperature at inlet	Temperature	100 ºC
Temperature at exit	Temperature	153 ºC
Initial Temperature	Initial Condition	20ºC

The flow boundary condition used are: Flow input and outlet :22 kg/hr

The meshed model and the FE model are shown in Figures 47 and 48 below:

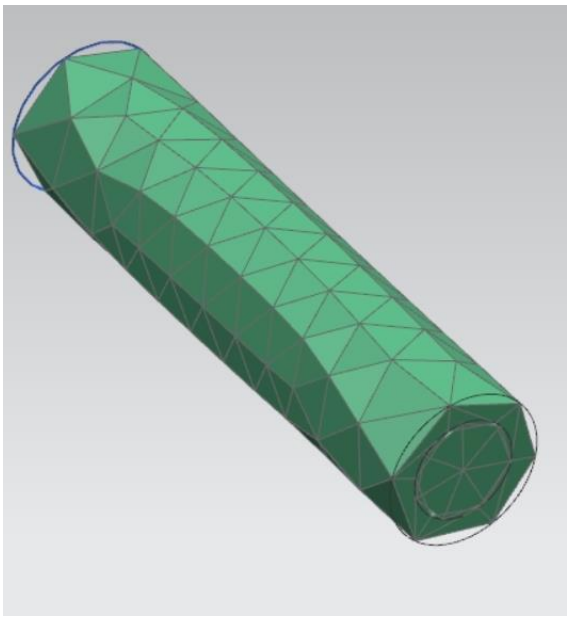

Figure 46) Meshed Model of Single Tube of Heat Exchanger

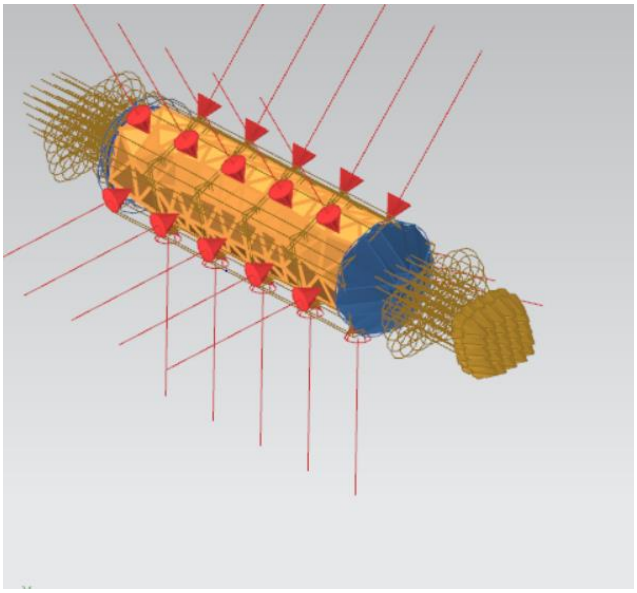

Figure 47) Model of single tube of heat exchanger

Table 9 lists the Average Scale Information generated by the solver:

Table 9) Average Scale Information

Quantity	Scale
Global Length Scale	2.721 X 10^-2
Density Scale	1000
Dynamic Viscosity Scale	1.006 X 10^-3
Prandtl Number	6.985
Cp Scale	4.187 X 10^3
Conductivity Scale	6.03 X 10^-1
Thermal Expansion Scale	1.82 X 10^-4

Convergence history for the different quantities at Time Step 1 and 17 are shown in Table 10 and Table 11. **Solution summary is shown in Table 12.**

Table 10) Convergence History at Time Step1

Equation	**Rate**	**RMS Res**	**Max Res**	**Location**	**Linear solution**
U-Momentum	0.00	0	0	0	0 OK
V -Momentum	0.00	0	0	0	0 OK
W-Momentum	0.00	2.5 X 10^-1	1	311	1.1 X 10^-3 OK
P-Mass	0.00	2.3 X 10^-2	7.5 X 10^-2	8	7.2 9.1 X 10^-2 OK
H-Energy	0.00	7.7 X 10^-10	2.4 X 10^-9	358	7.3 0 OK

Table 11) Convergence History at Time Step 17

Equation	**Rate**	**RMS Res**	**Max Res**	**Location**	**Linear solution**
U-Momentum	0.59	1 X 10^-5	3.8X10^-5	4	1 .1X10^-1 OK

Equation	Rate	RMS Res	Max Res	Location	Linear solution
V -Momentum	0.60	9.8 X10^-6	3.9 X10^-5	352	1 .3X10^-1 OK
W-Momentum	0.55	1.7 X10^-4	3.2X10^-4		
P-Mass	0.57	5.5 X10^-6	2.6 X10^-5	392	9.8 X10^-3 OK 7.2 3.1 X10^-2 OK
H-Energy	0.91	1.8 X10^-9	5.5 X10^-9	337	7.7 31.1X10^-1 OK

Table 12) Solution Summary

Maximum Temperature	153 ºC
Maximum Heat Transfer Coefficient	1.27 X 10^3 W/m^{2}ºC
Minimum Heat Transfer Coefficient	5.312 X 10^2 W/m^{2}ºC
Average Heat Transfer Coefficient	1.053 X 10^3 W/m^{2}ºC
Heat convected to fluid	-1.583 X 10^-6 W

Since the heat transfer calculated is very low, as per the solver an analytical calculation is done as below:

Enthalpy at condenser outlet, h_1=418.9 kJ/kg @ 100 ºC atmospheric pressure, as the condenser is not designed for vacuum exhaust, but has no back pressure.

A feed pump is used to add work to the system, at 75 PSI to encounter pressure drop issues in the system. Hence theoretically the heat addition in the boiler is designed for 75 PSI, which is the pump pressure and is isobaric.

Enthalpy at economizer outlet h_2=645.69 kJ/kg @ 153ºC, where saturated water is formed.

Enthalpy at evaporator outlet h_3=2749.61 kJ/kg @153ºC, where saturated steam is formed.

Heat transfer in economizer= BMCR X(h_2-h_1) = 6.927 kW

Heat transfer in evaporator =BMCR X(h_3-h_2) = 64 kW

Heat transfer in superheater= BMCR X(h_4-h_3) =9.792 kW

Thus, total heat transfer in boiler= 6.927+64+9.792=80.95 kW

The system is designed with input flue gas temperature from the combustor at 900ºC at inlet of economizer. The outlet temperature of flue gas after the entire heat transfer process is to be higher than the outlet steam temperature at 300ºC, so that the second law of thermodynamics is not violated. Thus 320ºC, is stipulated as the temperature of flue gas at outlet of the superheater section. **Figure 48 shows the temperature distribution of steam and flue gas in superheater, economizer and evaporator sections.**

$\dot{m}\, X(\mathrm{T_{G1}} - \mathrm{T_{G4}})\mathrm{X}\ \mathrm{C_P}$ heat transferred in boiler (14)

where $T_{G=}$ temperature of flue gas, suffix 1 indicates economizer inlet, 2 indicates, evaporator inlet, 3 indicates superheater inlet and 4 indicates superheater outlet and $\dot{m}$ is the mass flow rate in the flue gas path is calculated as 0.125 kg/s and C_p is the specific heat of flue gas mixture. T_{G1} =900ºC, T_{G4}=320ºC. Using the same equation for the individual temperature differences across the economizer, evaporator and superheater,

T_{G3} and T_{G4} are calculated as 850 ºC and 320ºC.

Calculations are done using the following basic equation to find U.

$$\frac{1}{\mathrm{UA}} = \mathrm{R_{TOTAL}} = \mathrm{R_{in}} + \mathrm{R_O} + \mathrm{R_{COND}} \quad (15)$$

Where, R_{in} = Convection resistance inside tube $= \frac{1}{\Pi * L * h_{in} D_{in}}$ (16)

UA= conductance (W)

L= length of tube (m)

D_{in}=Tube Inside Diameter (inch)

$$R_{out} = \text{convection resistance outside tube} = \frac{1}{h_{out} A_s} \quad (17)$$

$$R_{cond} = \frac{ln(\frac{D_{out}}{D_{in}})}{2\pi * k * L} \quad (18)$$

k=coefficient of thermal conductivity (W/m-K)

UA for the whole exchanger is calculated using, Q=(UA) LMTD (19)

Where LMTD=Log Mean Temperature Difference is calculated for a counter current heat exchanger as follows:

$$\text{LMTD} = \frac{[T_1 - t_2] - [T_2 - t_1)}{\ln(\frac{T_1 - t_2}{T_2 - t_1})} \quad (20)$$

Where, T is the hot fluid, t is for the cold fluid and suffixes 1 and 2 represent inlet and outlet.

Using the above equations, the LMTD, U (Overall Heat Transfer Coefficient and required surface area are selected. Velocities are selected from boiler design handbooks and HEI standards. For the superheater section, the tube velocity is selected as 35 ft/s, while for the economizer it is 6.6 ft/s. **Table 13 and 14 summarizes the results of the analytical study.**

Table 13) Result Sheet for Superheater and Economizer

Design Parameters	Value for Superheater	Value for Economizer	Units
Gas inlet (T_1)	389	900	C
Gas exit (T_2)	320	850	C
Steam in (t_1)	153	100	C

Design Parameters	Value for Superheater	Value for Economizer	Units
Steam out (t_2)	300	153	C
LMTD	124.3790041	750.3	
Conductance(UA)	0.086913203	0.009232668	kW/C
Film coefficient (outside) (h_{out})	5.596964366	0.0622	W/m^2 ° C
Area required	0.95 (with 5 % margin for plugging)	9.77 (with 5 % plugging margin)	m^2
Area provided	1.1.34	10.5	m^2
Velocity in tube	35	6.69	ft/s
No of tubes in superheater	5	24 (6 rows, 4 columns)	
Tube Inner Diameter X Length	0.65 X 39	3.27 X 39	Inch

Table 14) Results for Evaporator

Parameter	Value	Unit	Variable
Hot Gas Inlet	850.3640795	C	T1
Hot gas exit temperature	389.7114279	C	T2
Water in	153	C	t1
Steam out	153	C	t2
LMTD	426.3463391		
Conductance	UA=Heat Transfer/(LMTD)	0.167548247	kW/C

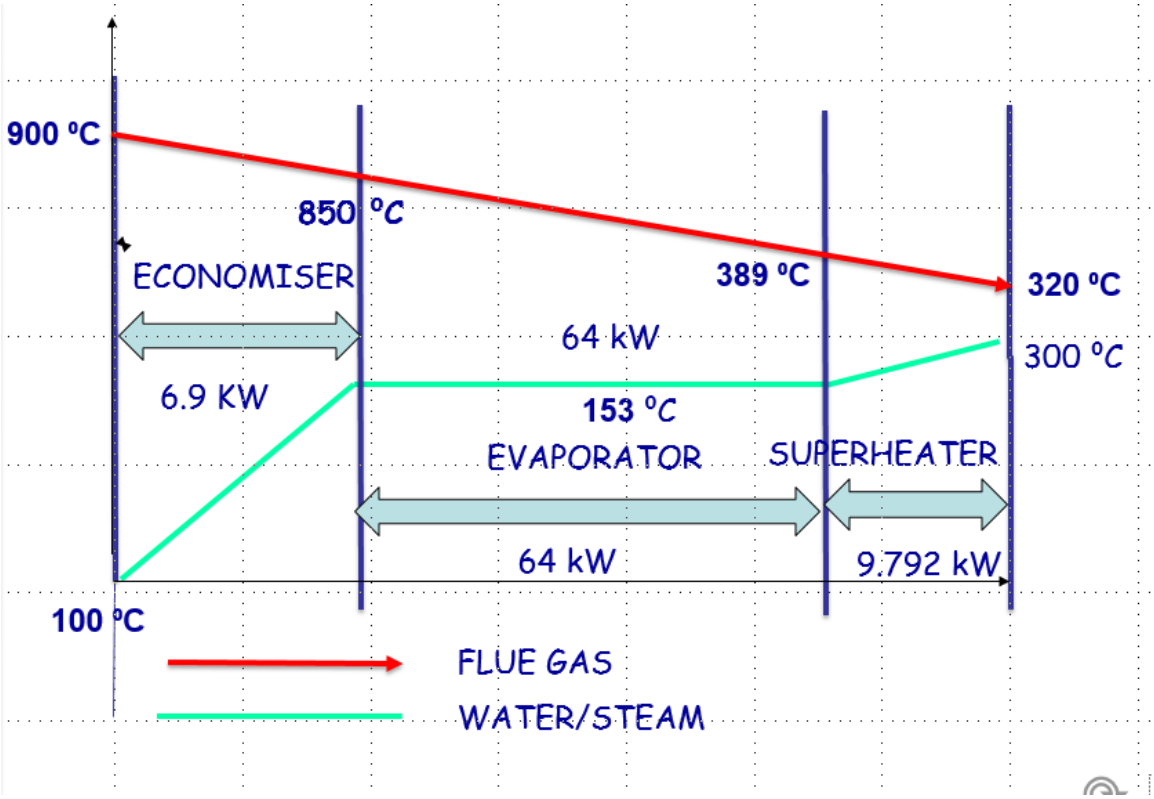

Figure 48) Temperature Distribution of Steam and Flue Gas at different stages of the Heat Exchange Process

CHAPTER SIX: CONCLUSIONS

The heat exchanger is designed for a flow rate of 110 kg/hr to feed an engine input thermal power of 75 kW. The main challenges faced in the engineering of the steam system and its solutions are as follows:

a. The system shall have a quick start up boiler. This is because unlike an industrial boiler, a vehicle shall be able to start instantly. There is no time for prolonged start-up as in case of industrial power generation boilers. Thus, an alternative drive like a battery system shall be used in this vehicle, till the boiler starts.

b. Another problem of the steam boilers in vehicles historically have been the fire tube design which leads to slower start up as well as greater risk. Hence in this case the water and steam will flow through tubes of SS 304 while the flue gas generated by combustion of natural gas, will be on the outside. The system must be properly insulated to prevent loss of heat from the gas stream. The fire tube design is not selected as it is inherently dangerous and has led to more accidents in steam boilers. So, a water tube design is chosen, with layers of insulation and cladding on the outside of the Mild Steel Shell of the heat exchanger and combustion chamber.

c. The system is designed using a coupled steady state thermal flow analysis, where the equations of conservation of mass, energy and momentum are used. The Siemens NX

thermal flow solver is used to analyze the heat transfer of straight tube. The boundary conditions are temperature at inlet, outlet and mass flow rate. A first order advection scheme is used and the k-epsilon turbulent scheme is used. The results reveal a maximum heat transfer coefficient of 1.27 X 10^3 $W/m^{2o}C$ and a minimum heat transfer coefficient of 5.312 X 10^2 $W/m^{2o}C$. These results are of the economizer section. However, the solver gives a very low value of heat transfer in the economizer section of 1.583 X10^-6 W, for one tube. Hence analytical calculations are done to get a better idea.

d. The resistances to heat transfer were calculated for internal convection with water, external convection with air flowing around a cylinder and the conduction resistance along the tube walls. The LMTD method was used to calculate, the required surface area for heat transfer for the superheater and economizer stages. 3.27 inch and 0.65 inch are the inner diameters selected for the economizer and superheater sections, while the length of tube in both sections in 39 inch. Thus, the boiler is compact and shall meet the requirements of a steam vehicle,

LIST OF REFERENCES

1. Taylor, C.F., *The Internal-combustion Engine in Theory and Practice: Combustion, fuels, materials, design*. Vol. 2. 1985: MIT press.
2. Granovskii, M., I. Dincer, and M.A. Rosen, *Economic and environmental comparison of conventional, hybrid, electric and hydrogen fuel cell vehicles.* Journal of Power Sources, 2006. **159**(2): p. 1186-1193.
3. Chan, C.C., *The state of the art of electric, hybrid, and fuel cell vehicles.* Proceedings of the IEEE, 2007. **95**(4): p. 704-718.
4. Ogden, J.M., M.M. Steinbugler, and T.G. Kreutz, *A comparison of hydrogen, methanol and gasoline as fuels for fuel cell vehicles: implications for vehicle design and infrastructure development.* Journal of power sources, 1999. **79**(2): p. 143-168.
5. Weaving, J.H. *The Austin Vehicle Gas Turbine*. in *ASME 1957 Gas Turbine Power Conference*. 1957. American Society of Mechanical Engineers.
6. Strack, W., *Condensers and Boilers for Steam-powered Cars.'.* NASA Technical Note, TN D-5813, Washington, DC, 1970.
7. Li, J., et al., *Energetic and exergetic investigation of an organic Rankine cycle at different heat source temperatures.* Energy, 2012. **38**(1): p. 85-95.
8. Badami, M. and M. Mura, *Preliminary design and controlling strategies of a small-scale wood waste Rankine Cycle (RC) with a reciprocating steam engine (SE).* Energy, 2009. **34**(9): p. 1315-1324.

9. Anthony, S. *Are Steam Cars Poised for an Epic comeback*. February 18, 2013; Available from: http://www.extremetech.com/extreme/148416-are-steam-cars-poised-for-an-epic-comeback.

10. *Steam Engine*. Available from: https://www.britannica.com/technology/steam-engine.

11. *Stanley Steamer*. Available from: http://www.stanleysteamers.com/.

12. Abram, T. and S. Ion, *Generation-IV nuclear power: A review of the state of the science.* Energy Policy, 2008. **36**(12): p. 4323-4330.

13. Almanza, R. and A. Lentz, *Electricity production at low powers by direct steam generation with parabolic troughs.* Solar Energy, 1998. **64**(1): p. 115-120.

14. Zhang, N., et al., *3D CFD simulation of hydrodynamics of a 150MW e circulating fluidized bed boiler.* Chemical Engineering Journal, 2010. **162**(2): p. 821-828.

15. Howell, J., M. Hall, and J. Ellzey, *Combustion of hydrocarbon fuels within porous inert media.* Progress in Energy and Combustion Science, 1996. **22**(2): p. 121-145.

16. Mujeebu, M.A., et al., *Applications of porous media combustion technology–a review.* Applied Energy, 2009. **86**(9): p. 1365-1375.

17. Delalic, N., D. Mulahasanovic, and E. Ganic, *Porous media compact heat exchanger unit—experiment and analysis.* Experimental Thermal and Fluid Science, 2004. **28**(2): p. 185-192.

18. Malico, I., X. Zhou, and J. Pereira, *Two-dimensional numerical study of combustion and pollutants formation in porous burners.* Combustion science and technology, 2000. **152**(1): p. 57-79.

19. Wood, S. and A.T. Harris, *Porous burners for lean-burn applications.* Progress in Energy and Combustion Science, 2008. **34**(5): p. 667-684.

20. Henríquez-Vargas, L., M. Valeria, and V. Bubnovich, *Numerical study of lean combustibility limits extension in a reciprocal flow porous media burner for ethanol/air mixtures.* International Journal of Heat and Mass Transfer, 2015. **89**: p. 1155-1163.

21. Hoffmann, J., et al., *Experimental study on combustion in porous media with a reciprocating flow system.* Combustion and flame, 1997. **111**(1): p. 32-46.

22. Wang, H., et al., *Experimental study on temperature variation in a porous inert media burner for premixed methane air combustion.* Energy, 2014. **72**: p. 195-200.

23. Avdic, F., M. Adzic, and F. Durst, *Small scale porous medium combustion system for heat production in households.* Applied Energy, 2010. **87**(7): p. 2148-2155.

24. Bhutta, M.M.A., et al., *CFD applications in various heat exchangers design: A review.* Applied Thermal Engineering, 2012. **32**: p. 1-12.

25. Ozden, E. and I. Tari, *Shell side CFD analysis of a small shell-and-tube heat exchanger.* Energy Conversion and Management, 2010. **51**(5): p. 1004-1014.

26. Rennie, T.J. and V.G. Raghavan, *Numerical studies of a double-pipe helical heat exchanger.* Applied Thermal Engineering, 2006. **26**(11): p. 1266-1273.

27. Rennie, T.J. and V.G. Raghavan, *Experimental studies of a double-pipe helical heat exchanger.* Experimental Thermal and Fluid Science, 2005. **29**(8): p. 919-924.

28. Van Der Vyver, H., J. Dirker, and J.P. Meyer. *Validation of a CFD model of a three-dimensional tube-in-tube heat exchanger*. in *Proceedings of Third International Conference on CFD in the Minerals and Process Industries, CSIRO, Melbourne, Australia*. 2003.

29. Kumar, V., et al., *Pressure drop and heat transfer study in tube-in-tube helical heat exchanger.* Chemical Engineering Science, 2006. **61**(13): p. 4403-4416.

30. Kang, H., C.-X. Lin, and M. Ebadian, *Condensation of R134a flowing inside helicoidal pipe.* International journal of heat and mass transfer, 2000. **43**(14): p. 2553-2564.

31. Naphon, P. and S. Wongwises, *A review of flow and heat transfer characteristics in curved tubes.* Renewable and sustainable energy reviews, 2006. **10**(5): p. 463-490.

32. Prabhanjan, D., G. Raghavan, and T. Rennie, *Comparison of heat transfer rates between a straight tube heat exchanger and a helically coiled heat exchanger.* International Communications in Heat and Mass Transfer, 2002. **29**(2): p. 185-191.

33. Prabhanjan, D.G., T.J. Rennie, and G.V. Raghavan, *Natural convection heat transfer from helical coiled tubes.* International Journal of Thermal Sciences, 2004. **43**(4): p. 359-365.

34. Jayakumar, J., et al., *Experimental and CFD estimation of heat transfer in helically coiled heat exchangers.* chemical engineering research and design, 2008. **86**(3): p. 221-232.

35. Nariai, H., M. Kobayashi, and T. Matsuoka, *Friction pressure drop and heat transfer coefficient of two-phase flow in helically coiled tube once-through steam generator for integrated type marine water reactor.* Journal of Nuclear Science and Technology, 1982. **19**(11): p. 936-947.

36. Gómez, A., N. Fueyo, and L.I. Díez, *Modelling and simulation of fluid flow and heat transfer in the convective zone of a power-generation boiler.* Applied Thermal Engineering, 2008. **28**(5): p. 532-546.